Published in Physical Chemistry Chemical Physics 2005, vol 7, p 3331-33-41
DOI: 10.1039/b505890b reprints also to galceran@quimica.udl.cat

LBGK method coupled to time splitting technique for solving reaction-diffusion processes in complex systems

Davide Alemani,[a] Bastien Chopard,[b] Josep Galceran,[c] Jacques Buffle,[a,*]

[a] CABE Department, University of Geneva, Switzerland
[b] CUI Department, University of Geneva, Switzerland
[c] Chemistry Department, University of Lleida, Spain
[*] Corresponding author: Jacques.Buffle@cabe.unige.ch

A new approach to numerically solve a reaction-diffusion system is given, specifically developed for complex systems including many reacting/diffusing species with broad ranges of rate constants and diffusion coefficients, as well as complicated geometry of reacting interfaces. The approach combines a Lattice Boltzmann (LB) method with a splitting time technique. In the present work, the proposed approach is tested by focusing on the typical reaction process between a metal ion M and a ligand L, to form a complex ML close to the electrode interface with the aim of systematically studying the convergence conditions of the numerical scheme associated. We find that the combination of LB with time splitting method allows us to solve the problem for any value of association and dissociation rate constant of the reaction process. Also, the method can be extended to a mixture of ligands. We stress two main points: 1) the LB approach is particularly convenient for the flux computation of M and 2) the splitting time procedure is very well suited for reaction processes involving association-dissociation rate constants varying on many orders of magnitude.

1 Introduction

In many environmental and industrial processes involving interfacial phenomena, it is very important to know the value of the flux of key species (e.g. metal ions) which cross the interface [1]. These processes appear in a variety of situations ranging from cellular nutrition and bio-ouptake of pollutants by micro-organisms to analytical instrumental measurements [2]. The development of numerical simulations of these types of processes is therefore important. In this paper we will introduce a new numerical approach for computing the metal ion fluxes, based

Published in Physical Chemistry Chemical Physics 2005, vol 7, p 3331-33-41
DOI: 10.1039/b505890b reprints also to galceran@quimica.udl.cat

on a Lattice Boltzmann (LB) numerical scheme combined with a time splitting method. Without any loss of generality in the applications, we adhere to the nomenclature in electrochemistry, and the discussion will be based on the typical problem:

$$\mathrm{M}^0 \overset{ne^-}{\rightleftharpoons} \mathrm{M} + \mathrm{L} \underset{k_a}{\overset{k}{\rightleftharpoons}} \mathrm{ML} \tag{1}$$

where L is a ligand and M is a cation reduced into M^0 with n electrons at the electrode surface. Other charges are omitted for the sake of simplicity. The main purpose of the paper is to investigate the capabilities of the Lattice Boltzmann method, (the so-called LB approach; see [3] and the references quoted for a synthetic and complete introduction) coupled to the splitting time method (see [4] for a complete introduction to the splitting methods applied to reaction-diffusion problems), for solving numerically this type of problem in complicated systems (see below).

Usually, processes like (1) are numerically solved by applying the finite difference approach or the multigrid technique [6], the finite element method [7, 8] or the boundary element method [9]. When analytical expressions are pursued, the work is restricted to the excess of ligand case, which mathematically corresponds to the simpler linear case. However, the aforementioned approaches are not applicable to environmental or biological systems which most often include i) very complicated interfacial geometry (e.g. porous media) and ii) **a** mixture of a very large number of ligands L_i with rate constants and diffusion coefficients ranging over many orders of magnitude. It is expected that LB coupled to splitting techniques will be very efficient numerical methods for solving such systems. This paper, as a first step, will focus mainly on their application to the simple system (1), even though the case of mixture of ligands is briefly discussed.

In the last decade, the LB approach have met significant success in simulating a wide range of phenomena (for instance, many applications can be found in [10]), involving reaction-diffusion systems (good examples are [11] and [12]). The major advantage of these methods over traditional numerical techniques, is that they provide insight into the underlying microscopic dynamics of the physical system investigated, whereas most methods focus only on the solution of the macroscopic equations [12]. For instance, we will show a 'natural' way to compute the flux by using microscopic functions, which avoids the calculation of the gradient of macroscopic functions. On the other hand, LB has not yet been extensively used in this field, because it has no major advantage for systems with only one or two reactions like (1) and for simple geometry which are the large majority of cases reported in the literature up to now.

The time splitting method is a classical technique, first introduced by Yanenko [13], to solve problems involving several physical and chemical processes taking place at different time scales with widely varying rate constants. As mentioned above, this is a major feature of environmental and biological systems. Many authors have already applied splitting methods to

Published in Physical Chemistry Chemical Physics 2005, vol 7, p 3331-33-41
DOI: 10.1039/b505890b reprints also to galceran@quimica.udl.cat

reaction-diffusion systems [14], where different time scales need to be resolved, and to dynamic systems ([5],[15] and [16]) where a suitable statistical description of the phenomena is required for the large number of unknowns involved. To our knowledge, the splitting technique, however, has never been coupled to the LB approach and this paper studies the optimum conditions for doing this.
This paper has two main goals:

1. To systematically study the capability of the time splitting LB method , to compute the transient flux of a metal ion M which can react in solution with many ligands and which is consumed on a surface, as exemplified by the prototype problem (1).

2. To write a numerical code to solve the prototype problem (1) for any concentration of ligand L, with the possibility of extending this code to mixture of ligands and complicated geometries.

2 The physical problem

As shown in figure 1, the metal ion M in solution can form a complex ML with a ligand L via reaction (1), with equilibrium constant K and association and dissociation rate constants k_{a} and k_{d}. M, ML and L diffuse in solution with diffusion coefficients D_{M}, D_{ML} and D_{L}. In the plane $x = 0$ an electrode is placed allowing M to be reduced into the metal species M^0 via the redox reaction $\mathrm{M}+\mathrm{ne}^- \leftrightharpoons \mathrm{M}^0$, when a sufficiently negative potential E is applied. M^0 diffuses inside the electrode with diffusion coefficient D_{M^0}, by forming an amalgam, e.g. like in Hg electrodes. Note that the case where the reduced form of M diffuses in the same solution is straightforward.
Two key parameters must be introduced here: the diffusion layer thickness δ and the reaction layer thickness μ. The diffusion layer can be understood for each species as the region in the vicinity of an electrode where the concentration is significantly different from its bulk value. The value of the diffusion layer thickness depends on voltammetric conditions. However, in many cases, δ_{X}, can be expressed as [21]:

$$\delta_{\mathrm{X}} = \sqrt{\pi D_{\mathrm{X}} t} \tag{2}$$

where X is the diffusive species and t is the total time in which diffusion occurs.
The reaction layer thickness μ can be understood as the distance from the electrode surface beyond which the deviation from the chemical equilibrium is taken to be negligibly small. Outside this layer, when M dissociates from ML, it can be only recombined to L after some short time. Inside this layer, the dissociated M can either recombine to L or move and be

Published in Physical Chemistry Chemical Physics 2005, vol 7, p 3331-33-41
DOI: 10.1039/b505890b reprints also to galceran@quimica.udl.cat

reduced at the electrode surface. The thickness μ is defined as [21]:

$$\mu = \sqrt{\frac{D_{\mathrm{M}}}{k_{\mathrm{a}} c_{\mathrm{L}}^{*}}} \tag{3}$$

where c_{L}^{*} is the bulk concentration of L. For fast reactions (k_{a} large), this distance is a very thin layer. For intermediate k_{a} values, the rate of the chemical reaction of interest, play an important role on the flux of the metal ion M towards the interface at $x = 0$. The thicknesses of δ and μ influence the numerical simulation of the reaction-diffusion process by playing a crucial role in the choice of the value of discretization parameters Δx. In general, Δx has to be less than the minimum value taken by either μ or δ in order to be able to resolve the concentration gradients of all the species, close to the electrode surface.
The selected geometry in this work corresponds to planar diffusion, which is also adequate to describe diffusion at a spherical electrode, provided the sphere radius is large compared to δ and the time domain of interest is small enough. For instance, for a spherical electrode of radius r_0, the planar diffusion is accurate within $a\%$ if $\frac{\delta}{r_0} \leq \frac{a}{100}$.
The planar semi-infinite diffusion-reaction problem is described by the following system of partial differential equations in the x-axis, $\forall t > 0$:

$$\frac{\partial c_{\mathrm{M}}}{\partial t} = D_{\mathrm{M}} \frac{\partial^2 c_{\mathrm{M}}}{\partial x^2} + R \tag{4}$$

$$\frac{\partial c_{\mathrm{ML}}}{\partial t} = D_{\mathrm{ML}} \frac{\partial^2 c_{\mathrm{ML}}}{\partial x^2} - R \tag{5}$$

$$\frac{\partial c_{\mathrm{L}}}{\partial t} = D_{\mathrm{L}} \frac{\partial^2 c_{\mathrm{L}}}{\partial x^2} + R \tag{6}$$

$$\frac{\partial c_{\mathrm{M}^0}}{\partial t} = D_{\mathrm{M}^0} \frac{\partial^2 c_{\mathrm{M}^0}}{\partial x^2} \tag{7}$$

where

$$R = k_{\mathrm{d}} c_{\mathrm{ML}} - k_{\mathrm{a}} c_{\mathrm{M}} c_{\mathrm{L}} \tag{8}$$

Equations (4 - 6) are defined $\forall x \in (0, +\infty)$, while equation (7) is defined $\forall x \in (-\infty, 0)$. In order to compact the notation, we introduce the functions $c_{\mathrm{X}} = c_{\mathrm{X}}(x, t)$, with X=M, L, ML and M^0, which represent the values of the concentrations of the species involved in the processes.
The equilibrium constant, $K = \frac{k_{\mathrm{a}}}{k_{\mathrm{d}}}$ between the species of reaction (1) is defined by:

$$K = \frac{c_{\mathrm{ML}}^{*}}{c_{\mathrm{M}}^{*} c_{\mathrm{L}}^{*}} \tag{9}$$

Published in Physical Chemistry Chemical Physics 2005, vol 7, p 3331-33-41
DOI: 10.1039/b505890b reprints also to galceran@quimica.udl.cat

where c_{X}^{*} are the bulk concentrations of the species.
Initial conditions are the bulk values of c_{X}:

$$c_{\mathrm{X}} = c_{\mathrm{X}}^{*} \quad t = 0 \tag{10}$$

The boundary conditions of semi-infinite diffusion are the following:

$$c_{\mathrm{X}} \rightarrow c_{\mathrm{X}}^{*} \quad x \rightarrow \infty \tag{11}$$

For X=M^0 the infinity, in the boundary condition given by equation (11), has to be understood with the minus sign. Furthermore, the semi-infinite diffusion condition inside the amalgam is fulfilled only for electrode sizes much larger than $\sqrt{\pi D_{\mathrm{M}^0} t}$.
If ML and L are electroinactive there is no flux of ML and L crossing the electrode-solution interface ($x = 0, \forall t > 0$) :

$$\left(\frac{\partial c_{\mathrm{ML}}}{\partial x}\right)_{x=0} = 0 \tag{12}$$

$$\left(\frac{\partial c_{\mathrm{L}}}{\partial x}\right)_{x=0} = 0 \tag{13}$$

If a constant potential is applied at the electrode then, for a reversible redox process, the Nernst equation will be considered as one of the boundary conditions at the electrode-solution interface:

$$c_{\mathrm{M}}(t) = c_{\mathrm{M}^0}(t) e^{(E-E_0)nf} \quad \text{at } x = 0 \tag{14}$$

where n is the number of electrons involved in the redox reaction, E_0 is the standard redox potential for the couple M/M^0 and f is the Faraday reduced constant ($f = \frac{F}{RT} = 38.92V^{-1}$).
The remaining boundary condition comes from the flux conservation at the electrode surface:

$$D_{\mathrm{M}}\left(\frac{\partial c_{\mathrm{M}}}{\partial x}\right)_{x=0} = D_{\mathrm{M}^0}\left(\frac{\partial c_{\mathrm{M}^0}}{\partial x}\right) \tag{1 }$$

For simplicity, in the numerical simulations we will consider only problems where the potential $\Delta E = E - E_0 \ll -0.3V$ which allows to consider a perfect sink condition (also known as diffusion limited condition) for M and disregard equation (7) involving M^0.

3 The Numerical model

The Lattice Boltzmann (LB) method, stemming from the Boltzmann equation [22] has been successfully used in complex flow problem [18], reaction-diffusion systems [10, 3] and also wave propagation processes [10]. The LB approach is based on a mesoscopic description of the physical system. It assumes a discrete space characterised by a grid or a lattice of spacing Δx and a discrete time step of duration Δt. The lattice is identified by its spatial dimension d and

Published in Physical Chemistry Chemical Physics 2005, vol 7, p 3331-33-41
DOI: 10.1039/b505890b reprints also to galceran@quimica.udl.cat

its coordination number z indicating how many neighbours each lattice point has. Traditionally, the lattice is then referred to as a DdQz lattice (D stands for Dimension and Q for Quantities). The LB method is a particle based technique. Intuitively, it considers a dynamics of particles travelling on the lattice directions. These particles may interact when they meet at the same time on the same site. As a result, particles typically change their direction of motion or, in case of chemical reactions, can be transformed into another species. After the interaction, which is assumed to be instantaneous, particles jump to one of the neighbouring site, according to their new direction of motion. This propagation-collision process is then repeated as many time as desired.
Important quantities of a LB model are thus the microscopic velocities v_i, $i = 0, ..., z$, which denote the admissible velocities of the particles. The admissible velocities reflect the chosen lattice topology so that, in one time step, the particles can reach any of the z neighbouring lattice site. Conventionally, $v_0 = 0$ so as to allow for motionless particles.
The time evolution of a LB model is given in terms of the density distributions $f_i(x,t)$ which denote the density of particles entering a lattice site x at a discrete time t with microscopic velocity v_i, where i runs from 0 to z. From the f_i, the standard macroscopic quantities such as the local concentration density c, are obtained by:

$$c(x,t) = \sum_{i=0}^{z} f_i(x,t) \tag{16}$$

Therefore, in a LB approach, the description is finer than in a finite difference scheme as information on the particle microscopic velocity is included. An important consequence of this fact is that the f_i's also contain information on the spatial derivatives of the macroscopic quantities.
As explained above, the LB dynamics combines particle propagation and collision as follows:

$$f_i(x + v_i\Delta t, t + \Delta t) = f_i(x,t) + \Omega_i(f(x,t)) \tag{17}$$

The quantities Ω_i describe the interaction between the particles colliding at the same lattice site. Its specific expression varies according to the physical system which is modelled. Below we shall define it for a reaction-diffusion process.
A crucial ingredient of the collision term Ω_i is that it must preserve the conservation laws of the system. For instance, in a diffusion process, particle number is conserved and, in a fluid, momentum is also conserved.

3.1 The LBGK model for reaction-diffusion

We now focus the discussion on reaction-diffusion systems. The model we will use is the LBGK model, firstly introduced by Bhatnagar-Gross-Krook [23]. LBGK models are LB models in

Published in Physical Chemistry Chemical Physics 2005, vol 7, p 3331-33-41
DOI: 10.1039/b505890b reprints also to galceran@quimica.udl.cat

which the collision term Ω_i is expressed as a relaxation towards a given local equilibrium function f_i^{eq} which depend only on the local values of the macroscopic quantities (typically the concentration in reaction-diffusion systems).
Such a method has already been used for solving problems such as (4) - (7) (see for instance [3, 11, 12]). Its major advantages are that i) the LBGK model is very simple and easy to establish for reaction-diffusion systems, even in the presence of a large number of species and complicated boundary geometries, ans ii) the time step is limited only by accuracy and not by stability requirements [3]. Finally, the computer code is rather simple and not extensively time-consuming.
Here we consider DdQ$2d$ lattices which means a cubic-like lattice in dimension d in which each lattice site has $2d$ neighbours (that is we exclude the possibility of particles at rest). In $3D$, the lattice velocities are therefore: $v_1 = (0, 0, v)$, $v_2 = (0, v, 0)$, $v_3 = (v, 0, 0)$, $v_4 = (0, 0, -v)$, $v_5 = (0, -v, 0)$, $v_6 = (-v, 0, 0)$, where

$$v = \Delta x/\Delta t \tag{18}$$

The chemical species X=M, L, ML and M^0, are described by density distribution functions $f_{i,\mathrm{X}}(x,t)$. According to the general method, the macroscopic concentrations $c_{\mathrm{X}}(x,t)$ are then given by:

$$c_{\mathrm{X}}(x,t) = \sum_{i=1}^{2d} f_{i,\mathrm{X}}(x,t) \tag{19}$$

Following the general procedure of the LB method, equations (4) - (7) can be represented as follows:

$$f_{i,\mathrm{X}}(x + v_i\Delta t, t + \Delta t) = f_{i,\mathrm{X}}(x,t) + \Omega_{i,\mathrm{X}}^{\mathrm{NR}} + \Omega_{i,\mathrm{X}}^{\mathrm{R}} \tag{20}$$

where $\Omega_{i,\mathrm{X}}^{\mathrm{NR}}$ contains the non-reactive part of the interaction (e.g. diffusion) whereas $\Omega_{i,\mathrm{X}}^{\mathrm{R}}$ contains all chemical reactions affecting species X.
It can be shown [10, 3] that equations (4) - (7) are obeyed by $c_{\mathrm{X}} = \sum_i f_{i,\mathrm{X}}(x,t)$ provided that the collision operators are adequately chosen.
The non reactive operator $\Omega_{i,\mathrm{X}}^{\mathrm{NR}}$ is given as [3]:

$$\Omega_{i,\mathrm{X}}^{\mathrm{NR}} = \omega_{\mathrm{X}}(f_{i,\mathrm{X}}^{eq} - f_{i,\mathrm{X}}) \tag{21}$$

where we have droped the space and time coordinates x and t. The quantity ω_{X} is a free parameter that is related to the transport coefficients.
The reactive operator $\Omega_{i,\mathrm{X}}^{\mathrm{R}}$ is defined as [11]

$$\Omega_{i,\mathrm{X}}^{\mathrm{R}} = \pm\frac{\Delta t}{2d}R \tag{22}$$

Published in Physical Chemistry Chemical Physics 2005, vol 7, p 3331-33-41
DOI: 10.1039/b505890b reprints also to galceran@quimica.udl.cat

the sign is plus for X=M and L and minus for X=ML.
In case of a purely diffusive phenomenon, the relaxation parameter ω_{X} is related to the diffusion coefficients as [12]:

$$\omega_{\mathrm{X}} = \frac{2}{1 + 2d\frac{D_{\mathrm{X}}\Delta t}{\Delta x^2}} \tag{23}$$

In order to satisfy the mass conservation, the equilibrium function takes the following form [3, 16]:

$$f^{eq}_{i,\mathrm{X}}(x,t) = \frac{c_{\mathrm{X}}(x,t)}{2d} \tag{24}$$

To first order in the Chapman-Enskog expansion and in the limit $\Delta x \to 0$ and $\Delta t \to 0$, $\Delta x^2/\Delta t \to const$, the distribution functions in equation (20) are shown to obey [10, 16]:

$$f_{i,\mathrm{X}} = f^{eq}_{i,\mathrm{X}} + f^{neq}_{i,\mathrm{X}} \tag{25}$$

where

$$f^{neq}_{i,\mathrm{X}} = -\frac{\Delta t}{2d\omega_{\mathrm{X}}} v_i \cdot \nabla c_{\mathrm{X}}(x,t) \tag{26}$$

The above two equations establish the relationship between the macroscopical concentration c_{X} and the density distribution functions $f_{i,\mathrm{X}}$. Note that these expressions are valid only for pre-collision values.
The computation of the flux, $J_{\mathrm{M}} = -D_{\mathrm{M}}\nabla c_{\mathrm{M}}$ is straightforward, considering expression (26). By multiplying equation (26) by v_i and summing over i we obtain:

$$\sum_i f^{neq}_{i,\mathrm{M}} v_i = -\Delta t \frac{2d}{\omega_{\mathrm{M}}} 2v^2 \nabla c_{\mathrm{M}} \tag{27}$$

Here we have used the fact that, for a DdQ2d lattice, $\sum_i v_i v_i = 2v^2\mathbf{1}$,where $\mathbf{1}$ is the $d \times d$ identity matrix. Since, from equation (23)

$$D_{\mathrm{M}} = \frac{v^2\Delta t}{d}\Big(\frac{1}{\omega_{\mathrm{M}}} - \frac{1}{2}\Big)$$

we finally obtain

$$J_{\mathrm{M}} = -D_{\mathrm{M}}\nabla c_{\mathrm{M}} = \Big(1 - \frac{\omega_{\mathrm{M}}}{2}\Big)\sum_i f^{neq}_{i,\mathrm{M}} v_i = d\frac{\omega_{\mathrm{M}} D_{\mathrm{M}}}{\Delta x}\frac{1}{v}\sum_i f^{neq}_{i,\mathrm{M}} v_i \tag{28}$$

This expression is purely local and can be computed without having to discretize the concentration gradient. This feature is an interesting advantage of the LB approach. Note also that in case of a diffusive system, we have $\sum_i f^{eq}_{i,\mathrm{M}} v_i = 0$ and thus $\sum_i f^{neq}_{i,\mathrm{M}} v_i = \sum_i f_{i,\mathrm{M}} v_i$.

Published in Physical Chemistry Chemical Physics 2005, vol 7, p 3331-33-41
DOI: 10.1039/b505890b reprints also to galceran@quimica.udl.cat

The expression (28) for J_{M} is valid in solution. Some care is needed when computing the flux of particles exactly at the electrode surface. An electrode surface is typically a boundary condition. Thus, all the f_i are not known and some of them must be computed according to the desired behaviour at the boundary. In order to use equation (28), the missing f's must be set up consistently with the theory, that is we have to update the f_i's values at the boundary as shown in section 3.3. However, the amount of particles that is consumed at the electrode surface can always be computed directly from the balance between the number of particles reaching the electrode and those leaving it per time unit.

3.2 The Time Splitting Method in LBGK framework

The numerical scheme (20) is second order accurate and valid only when the time step of integration Δt is sufficiently small with respect to the association-dissociation reaction times. Indeed, one can discriminate two different time scales: the time scale of diffusion and that of reaction.
Our purpose is to perform simulations in a wide range of values of the (pseudo) first order rate constants $k_{\mathrm{a}}c_{\mathrm{L}}$ and k_{d}, typically between $10^{-5}s^{-1}$ and $10^{8}s^{-1}$, with usually $K' = \frac{k_{\mathrm{a}}c_{\mathrm{L}}}{k_{\mathrm{d}}} \gg 1$, i.e. under conditions where the complex has a major contribution to the flux.
The time scale of diffusion Δt_{D}, defined as $\Delta t_{\mathrm{D}} \sim \frac{\Delta x^2}{D_{\mathrm{M}}}$, is usually in the range from ms to s, while the reaction time scale is given by:

$$\Delta t_{\mathrm{K}} = \frac{1}{k_{\mathrm{a}}c_{\mathrm{L}}} \tag{29}$$

and ranges between ns and hours.
Roughly speaking the time splitting method is needed when $\Delta t_{\mathrm{K}} << \Delta t_{\mathrm{D}}$. For instance, let us consider a system with $k_{\mathrm{a}}c_{\mathrm{L}} = 10^{6}s^{-1}$ and $D_{\mathrm{M}} = 10^{-10}m^2/s$. The reaction time Δt_{K} is of the order of μs. If the diffusion time is of the order of ms, for equation (20) to be valid, the time step of integration Δt must be less than $\Delta t_{\mathrm{K}} = 10^{-6}$s. For a system with the same diffusion time but a faster reaction $k_{\mathrm{a}}c_{\mathrm{L}}^{*} = 10^{8}s^{-1}$, the time step of integration must be less than 10^{-8}s. Such a low value of integration time is not reasonable due to the very high computational CPU time required and, so, another method is needed to overcome this difficulty.
In cases where very different time scales occur, the time splitting method is very convenient.
We will outline below a numerical scheme which makes use of the time splitting method whitin the framework of the LBGK scheme (20). Therefore, from now on, equation (20) will be called the NS scheme, i.e. No-Split scheme in order to distinguish it from the splitting scheme that will be defined below.
The idea of the splitting method is to solve separately the diffusion and the reaction parts. This will produce extra integration errors (see appendix A.1) but will allow us to deal efficiently with a large difference in the characteristic time scales.

Published in Physical Chemistry Chemical Physics 2005, vol 7, p 3331-33-41
DOI: 10.1039/b505890b reprints also to galceran@quimica.udl.cat

For simplicity, we shall use the splitting technique directly at the level of the partial differential equations so as to build two coupled problems. The original problem is

$$\frac{\partial c}{\partial t} = T_{\mathrm{D}} c + T_{\mathrm{R}} c \tag{30}$$

where T_{D} and T_{R} are the diffusion and the reaction operators, respectively. We want to compute $c(t+\Delta t)$ by solving (30) on the time domain $[t, t+\Delta t]$ with the initial condition $c(t) = c_t$. By using the standard time splitting method, equation (30) is decomposed into

$$\frac{\partial c'}{\partial t} = T_{\mathrm{D}} c' \qquad \text{on } (t, t+\Delta t] \qquad \text{with } c'(t) = c_t \tag{31}$$

$$\frac{\partial c''}{\partial t} = T_{\mathrm{R}} c'' \qquad \text{on } (t, t+\Delta t] \qquad \text{with } c''(t) = c'(t+\Delta t) \tag{32}$$

The final value is $c(t+\Delta t) = c''(t+\Delta t)$. This is the so-called RD splitting scheme.
In the present paper, we will consider two LB dynamics to solve this coupled system of equation, one for each process. Thus the complete numerical scheme (20) is now split into its pure diffusive and reactive parts in the following way:

$$\bar{f}_{i,\mathrm{X}}(x + v_i \Delta t, t + \Delta t) = \tilde{f}_{i,\mathrm{X}}(x, t + \Delta t) + \Omega^{NR}_{i,\mathrm{X}}(\tilde{f}(x, t + \Delta t)) \tag{33}$$

and

$$\tilde{f}_{i,\mathrm{X}}(x, t' + \Delta t_{\mathrm{K}}) = \tilde{f}_{i,\mathrm{X}}(x, t') + \Omega^{R}_{i,\mathrm{X}}(\tilde{f}(x, t')) \tag{34}$$

Here we have assumed that the time variable t' for the reaction equation runs faster than t, the time variable of the diffusion equation. This means that $\Delta t_{\mathrm{K}} << \Delta t$. In addition, the initial condition of equation (34) is $\tilde{f}(x, t' = t) = \bar{f}(x, t)$. A schematic description of the RD scheme is shown in the left hand side of figure 2.
The sub-problem (33) is a numerical initial-boundary-value problem involving only diffusion process, therefore it will be called process D. On the other hand, sub-problem (34) is a numerical initial value problem involving only a chemical reaction, therefore it will be called process R. In such a way, we can define several splitting procedures. In the paper we will consider four splittings: RD, DR, DRD and RDR. Two splittings are explained below, step-by-step, in more detail.
Notice that process R is an explicit scheme, because the values of $\Omega^{R}_{i,\mathrm{X}}$ are computed at the actual time level. However, the very advantage of the time splitting method, is the possibility of using different techniques for sub-problems (33) and (34) and to use different time integration steps. In fact, during the simulation the time step Δt has to be understood as the main integration time and when not explicitly specified it will be used for both schemes D and R. Furthermore, to really profit of the advantages of the splitting techniques, an implicit scheme,

Published in Physical Chemistry Chemical Physics 2005, vol 7, p 3331-33-41
DOI: 10.1039/b505890b reprints also to galceran@quimica.udl.cat

which warrants a larger stability region [4], should be used for the reaction process (34). In this case, equation (34), is replaced by:

$$\tilde{f}_{i,\mathrm{X}}(x_j, t' + \Delta t_{\mathrm{K}}) = \tilde{f}_{i,\mathrm{X}}(x, t') + \Omega^R_{i,\mathrm{X}}(\tilde{f}(x, t' + \Delta t_{\mathrm{K}})) \tag{35}$$

We will discuss quantitatively the advantages of the splitting for fast chemical reactions in section 4 and in the appendix.

DR splitting

DR splitting is defined in this way (see figure 2): in the time interval $[t, t + \Delta t]$, firstly we compute an intermediate function $f'_{i,\mathrm{X}}(x) = \tilde{f}_{i,\mathrm{X}}(x, t + \Delta t)$ by solving equation (34) with the initial condition $\tilde{f}_{i,\mathrm{X}}(x, t) = f_{i,\mathrm{X}}(x, t)$. Then, we compute the solution at $t + \Delta t$ by solving equation (33) in the time interval $[t, t + \Delta t]$, with the initial condition $\bar{f}_{i,\mathrm{X}} = f'_{i,\mathrm{X}}(x)$ and the appropriate boundary conditions. The solution at $t+\Delta t$ will be: $f_{i,\mathrm{X}}(x, t+\Delta t) = \bar{f}_{i,\mathrm{X}}(x, t+\Delta t)$.

DRD splitting

DRD splitting is defined as follows (see figure 2): in the time interval $[t, t + \Delta t/2]$ firstly we compute an intermediate function $f'_{i,\mathrm{X}}(x) = \bar{f}_{i,\mathrm{X}}(x, t + \Delta t/2)$ by solving the equation (33) with the appropriate boundary conditions and the initial condition $\bar{f}_{i,\mathrm{X}}(x, t) = f_{i,\mathrm{X}}(x, t)$. Then, in the time interval $[t, t+\Delta t]$, we compute another intermediate function $f''_{i,\mathrm{X}}(x) = \tilde{f}_{i,\mathrm{X}}(x_j, t+\Delta t)$ by solving the equation (34) with the initial condition $\tilde{f}_{i,\mathrm{X}}(x, t) = f'_{i,\mathrm{X}}(x)$. Finally, we compute the solution at $t + \Delta t$ by solving again the equation (33) in the time interval $[t + \Delta t/2, t + \Delta t]$ with the appropriate boundary conditions and the initial condition $\bar{f}_{i,\mathrm{X}}(x, t + \Delta t/2) = f''_{i,\mathrm{X}}(x)$. The solution at time $t + \Delta t$ is: $f_{i,\mathrm{X}}(x, t + \Delta t) = \bar{f}_{i,\mathrm{X}}(x, t + \Delta t)$. The splitting RDR is deduced in the same way, with the role of R and D exchanged.

3.3 Numerical boundary conditions for 1D case

We must also write the boundary conditions in terms of the density distribution functions defined in equation (19). In the following we consider specifically the 1D case which is enough for the applications shown in this paper. For this purpose, we use the same approach as that in [16]. The values of the density distribution functions not known at the boundary can be computed from the macroscopical boundary condition by using the expression (28) which is well suited for Neumann boundary conditions, i.e. when the flux is known at the boundary. This is the case, for instance, for the species L and ML for which the flux is nil at the electrode surface. A simpler expression, exact at any order, will be used for the Dirichlet boundary conditions:

$$f_{i,\mathrm{X}}(x, t) = c_{\mathrm{X}}(x, t) - \sum_{k \neq i} f_{k,\mathrm{X}}(x, t) \tag{36}$$

Published in Physical Chemistry Chemical Physics 2005, vol 7, p 3331-33-41
DOI: 10.1039/b505890b reprints also to galceran@quimica.udl.cat

Therefore, the boundary condition will be formulated as follows:

1. To obtain the boundary condition at $x = 0$, for M and M^0, conditions (14) and (15) must be transformed in terms of density distribution functions. By combining expression (36) with the Nernst condition (14) and equation (28) with the flux conservation equation (15) to write the gradient, we get:

$$f_{1,\mathrm{M}} + f_{2,\mathrm{M}} = (f_{1,\mathrm{M}^0} + f_{2,\mathrm{M}^0})e^{(E-E_0)nf}$$

$$\beta_{\mathrm{M}}(f_{1,\mathrm{M}} - f_{2,\mathrm{M}}) = \beta_{\mathrm{M}^0}(f_{1,\mathrm{M}^0} - f_{2,\mathrm{M}^0})$$

where $\beta_{\mathrm{M}} = \frac{\omega_{\mathrm{M}} D_{\mathrm{M}}}{\Delta x}$ and $\beta_{\mathrm{M}^0} = \frac{\omega_{\mathrm{M}^0} D_{\mathrm{M}^0}}{\Delta x_0}$, Δx and Δx_0 are the mesh sizes of the space in solution and inside the electrode, respectively. After some algebraic manipulation one gets:

$$f_{2,\mathrm{M}^0} = \frac{f_{1,\mathrm{M}^0}\left(\beta_{\mathrm{M}^0} - \beta_{\mathrm{M}} e^{(E-E_0)nf}\right) + 2 f_{2,\mathrm{M}} \beta_{\mathrm{M}}}{\beta_{\mathrm{M}} e^{(E-E_0)nf} + \beta_{\mathrm{M}^0}} \tag{37}$$

$$f_{1,\mathrm{M}} = (f_{1,\mathrm{M}^0} + f_{2,\mathrm{M}^0})e^{(E-E_0)nf} - f_{2,\mathrm{M}} \tag{38}$$

In our specific applications, we shall consider here only cases where $E \ll E_0$, i.e. where the electrode surface is a perfect sink for M. Therefore we do not need to compute the concentration of M^0 and the conditions stated by equations (37) and (38) can be reduced to the condition on M:

$$f_{1,\mathrm{M}} = -f_{2,\mathrm{M}} \tag{39}$$

2. The boundary conditions for ML and L, at $x = 0$, are easily recovered. By using equation (25), conditions (13) and (12) take the new form:

$$f_{1,\mathrm{L}} = f_{2,\mathrm{L}} \tag{40}$$

$$f_{1,\mathrm{ML}} = f_{2,\mathrm{ML}} \tag{41}$$

3. The bulk conditions for M, L, ML at $x \to \infty$, are obtained by combining equations (11) with equation (36):

$$f_{2,\mathrm{M}} = c^*_{\mathrm{M}} - f_{1,\mathrm{M}} \tag{42}$$

$$f_{2,\mathrm{L}} = c^*_{\mathrm{L}} - f_{1,\mathrm{L}} \tag{43}$$

$$f_{2,\mathrm{ML}} = c^*_{\mathrm{ML}} - f_{1,\mathrm{ML}} \tag{44}$$

Published in Physical Chemistry Chemical Physics 2005, vol 7, p 3331-33-41
DOI: 10.1039/b505890b reprints also to galceran@quimica.udl.cat

4 Numerical results

4.1 Definitions of errors

Several numerical simulations will be shown to prove the quality of the proposed methods: NS, DR, RD, DRD and RDR. First of all, we introduce the notation on the error formula and the analytical solutions used to compare our numerical results.
In absence of ligand, the numerical computations of the concentration profile of M, $c_{\mathrm{M}}(x,t)$, will be compared with the following analytical solution [24]:

$$u(x,t) = c^*_{\mathrm{M}} erf\Big(\frac{x}{2\sqrt{D_{\mathrm{M}}t}}\Big) \tag{45}$$

which holds for problem involving $\Delta E \ll -0.3V$, where M attains condition of perfect sink at the electrode interface, i.e. $c_{\mathrm{M}}(0,t) = 0$. In all the following simulations this condition is satisfied. The error in the L^2-norm is defined as:

$$\|c_{\mathrm{M}}(x,t) - u(x,t)\|_2 = \sqrt{\sum_{j=1}^{n_x} |c_{\mathrm{M}}(x_j,t) - u(x_j,t)|^2} \tag{46}$$

where n_x is the number of discretization points. The numerical computation of the flux J_{M} will be compared to the analytical solutions known in two limiting cases: the totally inert and fully labile complex in presence of excess of ligand. For the inert case the analytical solution is [24]:

$$J_{\mathrm{inert}} = c^*_{\mathrm{M}} \sqrt{\frac{D_{\mathrm{M}}}{\pi t}} \tag{47}$$

while for the fully labile case the analytical solution is [24]:

$$J_{\mathrm{labile}} = c^*_{\mathrm{M,tot}} \sqrt{\frac{\bar{D}_{\mathrm{M}}}{\pi t}} \tag{48}$$

where $\bar{D}_{\mathrm{M}} = \frac{D_{\mathrm{M}} c^*_{\mathrm{M}} + D_{\mathrm{ML}} c^*_{\mathrm{ML}}}{c^*_{\mathrm{M}} + c^*_{\mathrm{ML}}}$ and $c^*_{\mathrm{M,tot}} = c^*_{\mathrm{M}} + c^*_{\mathrm{ML}}$. The relative error will be computed by the formula:

$$\epsilon_r = \frac{|J_{\mathrm{M}} - J_{\mathrm{inert}}|}{J_{\mathrm{inert}}} \tag{49}$$

for the inert case and by:

$$\epsilon_r = \frac{|J_{\mathrm{M}} - J_{\mathrm{labile}}|}{J_{\mathrm{labile}}} \tag{50}$$

for the fully labile case.
In order to analyse the numerical results for a semi-labile complex, we will also compare the

Published in Physical Chemistry Chemical Physics 2005, vol 7, p 3331-33-41
DOI: 10.1039/b505890b reprints also to galceran@quimica.udl.cat

flux of M with its normalised analytical expression, computed by solving the problem in excess of ligand, in the Laplace domain [20]. The normalised flux is defined as the ratio between the current flux of M and the flux of M in solution with the same total amount of M but no ligand:

$$\Phi(t) = \frac{J_{\mathrm{M}}}{J_{\mathrm{M,no\ ligand}}} \tag{51}$$

The analytical expression of equation (51), which has been computed in [20] for perfect sink condition at the electrode surface of M, is:

$$\Phi(t) = \frac{\sqrt{\pi D_{\mathrm{M}} t}}{c^{*}_{\mathrm{M,tot}}} L^{-1}\left[\left(\frac{d\bar{c}_{\mathrm{M}}}{dt}\right)_{x=0}\right] \tag{52}$$

where L^{-1} denotes the Laplace inverse transform. The inverse transform has been numerically computed by applying the matlab-script INVLAP.M available on the web [25]. The relative error of the normalised flux is defined as:

$$\epsilon_r = \frac{|\Phi_n - \Phi|}{\Phi} \tag{53}$$

where Φ_n is the numerical flux computed with equation (51), where J_{M} is found with expression (28) and Φ is computed from equation (52).

4.2 Choice of the best numerical method based on the excess of ligand case

In this sub-section we analyse the numerical results obtained, in excess of ligand, by comparing the results obtained with the splitting procedures RD, DR, DRD and RDR with NS and, whenever possible, with the exact solutions, in order to choose the best numerical approach for further more complicated conditions.
Figure 3 shows that the absolute L^2-error, see equation (46), decreases with the number of iteration steps with a slope approximately equal to -1, indicating a first order convergence, up to 1000 iteration steps, for the NS scheme and all splitting schemes. In general we can say that all the schemes are sufficiently accurate with approximately the same absolute precision.
However the error depends on $\Delta t/\Delta x$ and K values, as shown in figure (4). In all plots the same step size was used for diffusion and reaction, i.e $\Delta t_{\mathrm{D}} = \Delta t_{\mathrm{K}}$. The numerical scheme associated with the reaction is solved by an explicit method, equation (34). In all plots we observe that the NS scheme is the most accurate and, within the splitting schemes, RD is the best. Furthermore, we observe that when K takes high values, $K > 10^3 m^3/mol$, then the NS scheme no longer holds and we have to use the splitting schemes.
Table 1 shows the computational costs of the different splitting procedures. The results shown

Published in Physical Chemistry Chemical Physics 2005, vol 7, p 3331-33-41
DOI: 10.1039/b505890b reprints also to galceran@quimica.udl.cat

in table 1 and the the better accuracy exhibited in general by the RD scheme for computing the flux, suggest that this scheme is the most appropriate numerical procedure for our purpose. Specifically, considering 1000 iterations, with $\Delta t_{\mathrm{D}} = \Delta t_{\mathrm{K}}$, on a Pentium 4 (CPU 2.80Ghz), the explicit RD and DR schemes take around 4 seconds, the explicit DRD and RDR take around 6 seconds and NS scheme takes around 3 seconds.
Table 2 and table 3, also, show the accuracy of the results for inert and labile complexes, obtained with the RD splitting scheme. Table 2 shows the error on the flux found with equation (49) for the inert case. In table 3 we show the error on the flux for the labile complex in excess of ligand, (50). We can see that the method is good and is working for time steps Δt much higher than the reaction time scale Δt_{K}.
Tables 4 and 5 report results obtained with RD and NS methods for the flux at electrolysis time, $t = 0.015s$ and $t = 0.5s$ respectively. They are compared with the exact values given by equation (52) for a wide range of dissociation rate constant. At low or intermediate values of dissociation rate constant, k_{d}, both numerical schemes show a good agreement with the analytical values, but when k_{d} becomes too large then the NS scheme fails to converge, while the RD splitting continues to give good results close to the exact ones. The numerical results obtained by the RD method, however do not converge completely to the exact values. For instance, in table 4 the last three values corresponding to k_{d} from $10^5 s^{-1}$ to $10^7 s^{-1}$ are the same and differ from the exact value by 6%. In table 5 the last two values, corresponding to $k_{\mathrm{d}} = 10^4 s^{-1}$ and $k_{\mathrm{d}} = 10^5 s^{-1}$ have the same problem. This discrepancy is due to the very small reaction layer thickness μ compared to the space mesh size Δx. Indeed, in order to follow the variation of the ML concentration profile, the mesh size Δx has to be of the same order of magnitude of μ or smaller. This is not the case for the results discussed above, where Δx is larger than μ, for the largest k_{d} values. Figure 5 shows the behaviour of the relative error on the flux, eq. (53), as a function of the ratio $\frac{\Delta x}{\mu}$ and of the equilibrium constant $K' = \frac{k_{\mathrm{a}}}{k_{\mathrm{d}}} c_{\mathrm{L}}$. It enables to choose the conditions under which this error is minimised. The simulations have been performed with the RD scheme. When the contribution of the complex becomes important ($K' > 1$) the error is negligible (order of a few percent) only if $\frac{\Delta x}{\mu} < 1$.

4.3 Checking the validity of the proposed numerical procedure in excess of ligand

As shown in figure 6, the LBGK method presented in this paper, combined with the splitting RD technique, reproduces very well the behaviour of a kinetically intermediate complex, which passes from an inert to a labile behaviour. At short times, $\delta_{\mathrm{M}} = \sqrt{\pi D_{\mathrm{M}} t}$ is very small, and there is no time for the complex ML to dissociate in the diffusion layer. Thus, the behaviour is that of an inert complex and the numerical results fit the exact solution for inert complexes, eq. (47). At very long times, δ has increased very much and complexes have plenty of time to dissociate in the diffusion layer. They behave as fully labile complexes and the numerical

Published in Physical Chemistry Chemical Physics 2005, vol 7, p 3331-33-41
DOI: 10.1039/b505890b reprints also to galceran@quimica.udl.cat

curves tend towards the exact solution for the labile limiting case, eq. (48). For intermediate times, both chemical kinetics and diffusion influence the flux.
Our results compare well with well-known systems already investigated in the literature. In particular, figure 7 shows the plot of the normalised flux, eq. (51), at the surface, computed respectively with the NS scheme (dash-dotted line), the RD scheme (dashed line) and with eq. (52) (circles). The graph covers fluxes for inert (short times), labile (long times) and kinetically intermediate cases. The values obtained with our numerical procedures are in perfect agreement with the literature data [20] obtained by an analytical solution (circles).
An important result must be emphasised: the excess of ligand case can always be numerically solved by the NS scheme (20) provided that the condition $\Delta t < 2(k_\mathrm{a} c_\mathrm{L}^*)^{-1}$ is fulfilled (see A.3). The advantage of the splitting procedure, however, is that the excess of ligand case is solved for any values of the association and dissociation rates constant k_a and k_d, for any value of the diffusion coefficients D_M and D_ML and *w*ithout restrictions on the integration time Δt. (Notice that we do not need to compare Δt with k_d^{-1} because we usually work with $Kc_\mathrm{L} > 1$ which implies $k_\mathrm{a}^{-1}c_\mathrm{L}^{-1} < k_\mathrm{d}^{-1}$ and therefore $\Delta t < k_\mathrm{a}^{-1}c_\mathrm{L}^{-1} < k_\mathrm{d}^{-1}$).
This result opens up the possibility to choose the most suitable numerical method to solve the reaction process with either an explicit, eq. (34), or an implicit, eq. (35), method. In particular, we can apply an implicit Euler method, eq. (35), which works for any value of the association-dissociation rate constants (see appendix A.3 for a detailed discussion).

4.4 Mixture of ligands in excess compared to M

The above results can be extended to the case of a mixture of ligands. Indeed, in case of h ligands, L_1, L_2,..., L_h, present in the solution, we have to deal with h reactions of the type:

$$\mathrm{M} + \mathrm{L}_i \underset{k_\mathrm{a}^{(i)}}{\overset{k_\mathrm{d}^{(i)}}{\rightleftharpoons}} \mathrm{ML}_i \tag{54}$$

which introduce in the process h reaction times of the order of $(k_\mathrm{a}^{(i)} c_{\mathrm{L}_i})^{-1}$. Therefore (see section A.3 in the appendix), to get convergence, the spectral radius of the iteration matrix is less than one only if

$$\Delta t < \min_i 2(k_\mathrm{a}^{(i)} c_{\mathrm{L}_i}^*)^{-1} \tag{55}$$

which means that the fastest reaction determines the time integration step to use. Again, by applying the splitting time procedure, we reach the conclusion that the spectral radius of the iteration matrix, for a process involving a mixture of ligands is always less than one and so no restriction on the time integration step is required. Figure 8 shows an example of flux computation by applying the RD scheme to two ligands L_1 and L_2 which can react with M, following reaction (54) with $h = 2$. The reaction involving L_1 is much faster than that involving

Published in Physical Chemistry Chemical Physics 2005, vol 7, p 3331-33-41
DOI: 10.1039/b505890b reprints also to galceran@quimica.udl.cat

L_2. This flux cannot be compared to an analytical solution as far as we know. However the plot of this flux, in figure 8, is reasonable, in particular when it is compared to the fluxes computed by equations (47) and (48) for the fully inert and fully labile complexes respectively. Indeed, considering the kinetics of the two complexes, we can expect ML_2 to be inert even at the largest tested time, whereas ML_1 will be labile at that time. So at long times, we expect a flux around a half of that we would obtain for two fully labile complexes. Indeed, at $t = 0.5$s the flux, assuming two fully labile complexes, is equal to $8 \cdot 10^{-9}$mol m^{-2}s^{-1}, while the computed flux is $4.1 \cdot 10^{-9}$mol m^{-2}s^{-1}. Figure 9 shows the so-called normalised concentration profiles near the electrode, for the same example as above, which correspond to the ratio c_X/c_X^* where X = M and X = ML_i, respectively. We can see that the complex ML_1 is almost completely consumed at the electrode surface, while ML_2 is not consumed at all (inert) because of its very low lability. Notice that the normalised concentration profile of ML_1 collapses with that of M for $x > \mu_1$.

4.5 Computation of flux without ligand excess

In the following, we are going to check the application of the numerical procedure in the absence of ligand excess for different initial values of the ligand concentration c_L^*. Figure 10 shows the flux of M at the electrode computed, with the RD scheme when the solution contains only one complex ML. The concentration profiles are plotted after 1000 iteration steps. Initial concentrations of M, L and ML are such that $c_{M,tot}^* = c_L^* = 0.02 mol/m^3$. Since there is no exact solution for this case, the results cannot be validated against an analytical solution but we have checked that $c_L + c_{ML} = c_{L,tot}$ at any point. They are reasonable and in agreement with expected results. Furthermore, we have also studied the capability of the method for a process involving two ligands, L_1 and L_2. Again, as in the example shown in figure 8, we are considering two reactions with very different time scales. The flux computed by applying the RD scheme is shown in figure 11. The reaction involving L_1 is much faster than that involving L_2, and thus (given the actual concentrations and diffusion coefficients) the major contribution to the flux J_M is expected from the complex ML_1. This is confirmed in figure 12, where the normalised concentration profiles of the species are plotted as a function of the distance from the electrode surface.

In figure 13 are shown (crosses and circles) the normalised concentration profiles studied in the literature (fig. 7 of [17]) with the Finite Element method, by using a a very small grid size ($\Delta x \sim \mu/1000$) close to the electrode surface. For comparison, figure 13 shows the results obtained, for the same system, with a time splitting procedure (full lines), by using $\Delta x = \mu$. Very close to the electrode, we observe a discrepancy, due to the fact that the grid size ($\Delta x = \mu$) is too large. For larger values, agreement is good. To reach a high accuracy in such systems, a grid refinement technique will have to be introduced in our LBGK - splitting scheme to enable precise computation near the electrode surface, where the space variation of the concentration profiles are very large. This will be the topic of another paper.

Published in Physical Chemistry Chemical Physics 2005, vol 7, p 3331-33-41
DOI: 10.1039/b505890b reprints also to galceran@quimica.udl.cat

5 Conclusions

The numerical schemes we have investigated and the numerical simulations performed shown that the time splitting method is a very favourable and advantageous technique which allows the numerical scheme to be convergent for any values of the association-dissociation rate constants. The most important conclusions are highlighted in figure 14. If we do not apply the splitting procedure, the condition on the time integration step, in excess of ligand, is:

$$\Delta t < \frac{2}{k_{\mathrm{a}} c_{\mathrm{L}}^{*}} \tag{56}$$

while, if we couple LB with the splitting RD, no restriction on the time step Δt is required. On the other hand, for fast complex, i.e. for k_{a} very large, the reaction layer thickness μ could become smaller than the space grid Δx and incorrect concentration profiles are obtained. To overcome this problem, a grid refinement technique will be developed in another paper.
Furthermore, by applying the Lattice Boltzmann method, the way to compute the flux, with expression (28) is very simple and in the convergence domain of the numerical scheme it gives good results with an accuracy of the order of a few percent.

Acknowledgements

The authors gratefully acknowledge support of this work by the Swiss National Foundation. Josep Galceran also thanks the support of this research by the Spanish Ministry of Education and Science (DGICYT: Project BQU2003-07587).

A Appendix: mathematical tools

In this appendix we will introduce the key mathematical tools to study the errors and the numerical procedure of the splitting time method combined with the Lattice Boltzmann approach. In particular we show that: i) the splitting procedure introduces an error proportional to Δt^2 if the diffusion coefficients are equal. In other cases the error is only proportional to Δt; ii) NS and RD schemes have different Δt constraints; iii) How to write explicitly the matrices of the numerical schemes, in presence of ligand excess.

A.1 Splitting errors: the RD scheme

Following [4], after having rewritten equations (4), (5), (6) and (7) in the compact form $\frac{\partial u}{\partial t} = T_{\mathrm{D}} u + T_{\mathrm{R}} u$, where T_{D} and T_{R} are respectively the diffusion and the reaction operators, the error

Published in Physical Chemistry Chemical Physics 2005, vol 7, p 3331-33-41
DOI: 10.1039/b505890b reprints also to galceran@quimica.udl.cat

between the exact solution u_e and the splitted solution u_s is [4]:

$$\|u_e - u_s\| \leq \frac{\Delta t}{2}[T_D, T_R]u_e(0) + O(\Delta t^2) \tag{57}$$

where $u_e(0)$ is the initial value of the exact solution (at t=0) and the square parenthesis indicates the commutator operation ($[A, B] = AB - BA$). For instance, the commutator for a system in excess of ligand, takes the following value:

$$[T_D, T_R] = \begin{pmatrix} 0 & k_d(D_M - D_{ML})\nabla^2 \\ k'_a(D_M - D_{ML})\nabla^2 & 0 \end{pmatrix} \tag{58}$$

from which we can deduce that, if $D_M = D_{ML}$, the splitting error is proportional to Δt^2 in excess of ligand. If $D_M \neq D_{ML}$, the splitting error is proportional to Δt.

A.2 A concrete example of excess of one ligand

The results shown in the previous sub-appendix, are based on the concrete form of each matrix and of each vector of the problem. Let us consider the reaction-diffusion of the prototype process (1) in the excess of ligand case, in the space domain $\Omega = [0, 1]$ discretized with n_x points. Boundary conditions at x=0, are i) perfect sink for M ($c_M(0, t) = 0$), ii) electroinactivity for ML, i.e. no flux, $\frac{\partial c_{ML}}{\partial x} = 0$ and iii) at x=1 conditions are those of bulk both for M and ML, $c_M(1, t) = c^*_M$ and $c_{ML}(1, t) = c^*_{ML}$. Therefore, we do not need the equations for L and M^0, since we are working in the excess of ligand case and under condition of perfect sink for M. Let us introduce the vector $u^n = (f^n_{1,M}, f^n_{2,M}, f^n_{1,ML}, f^n_{2,ML})^T$, where $f^n_{1,M} = (f^n_{1,M,1}, f^n_{1,M,2}, ..., f^n_{1,M,n_x})^T$ and so on for $f^n_{2,M}$, $f^n_{1,ML}$ and $f^n_{2,ML}$. The numerical boundary conditions are the following: $f^n_{1,M,1} = -f^n_{2,M,1}$, $f^n_{1,ML,1} = f^n_{2,ML,1}$, $f^n_{2,M,n_x} = c^*_M - f^n_{1,M,n_x}$ and $f^n_{2,ML,n_x} = c^*_{ML} - f^n_{1,ML,n_x}$.
In general the numerical scheme will take the following form:

$$\begin{pmatrix} A_{11} & A_{12} & 0 & 0 \\ A_{21} & A_{11} & 0 & 0 \\ 0 & 0 & A_{33} & A_{34} \\ 0 & 0 & A_{43} & A_{33} \end{pmatrix} \begin{pmatrix} f_{1,M} \\ f_{2,M} \\ f_{1,ML} \\ f_{2,ML} \end{pmatrix}^{n+1} = \begin{pmatrix} B_{11} & B_{12} & B_{13} & B_{13} \\ B^T_{12} & B^T_{11} & B^T_{13} & B^T_{13} \\ B_{31} & B_{31} & B_{33} & B_{34} \\ B^T_{31} & B^T_{31} & B^T_{34} & B^T_{33} \end{pmatrix} \begin{pmatrix} f_{1,M} \\ f_{2,M} \\ f_{1,ML} \\ f_{2,ML} \end{pmatrix}^{n} + \begin{pmatrix} G_1 \\ G_2 \\ G_3 \\ G_4 \end{pmatrix} \tag{59}$$

The entries of each matrix are represented by sub-matrix A_{ij}, which take different forms depending on the scheme considered. If the space is discretized with n_x points then the dimension of each sub-matrix is $n_x \cdot n_x$.

A.2.1 Complete scheme: matrices A and B

$$A_{11} = [1]_{n_x \cdot n_x} \quad A_{12} = diag(1, 0, ..., 0)_{n_x \cdot n_x} \quad A_{33} = A_{11} \quad A_{34} = -A_{12}$$

Published in Physical Chemistry Chemical Physics 2005, vol 7, p 3331-33-41
DOI: 10.1039/b505890b reprints also to galceran@quimica.udl.cat

$$A_{21} = diag(0, ..., 0, 1)_{n_x \cdot n_x} \quad A_{43} = A_{21}$$

$$B_{11} = \begin{pmatrix} 0 & . & . & 0 \\ 1 - \frac{\omega_{\mathrm{M}} + k_{\mathrm{a}}\Delta t}{2} & 0 & . & . \\ 0 & . & 0 & . \\ 0 & 0 & 1 - \frac{\omega_{\mathrm{M}} + k_{\mathrm{a}}\Delta t}{2} & 0 \end{pmatrix}_{n_x \cdot n_x}$$

$$B_{12} = \begin{pmatrix} 0 & . & . & 0 \\ \frac{\omega_{\mathrm{M}} - k_{\mathrm{a}}\Delta t}{2} & 0 & . & . \\ 0 & . & 0 & . \\ 0 & 0 & \frac{\omega_{\mathrm{M}} - k_{\mathrm{a}}\Delta t}{2} & 0 \end{pmatrix}_{n_x \cdot n_x}$$

$$B_{13} = \begin{pmatrix} 0 & . & . & 0 \\ \frac{k_{\mathrm{d}}\Delta t}{2} & 0 & . & . \\ 0 & . & 0 & . \\ 0 & 0 & \frac{k_{\mathrm{d}}\Delta t}{2} & 0 \end{pmatrix}_{n_x \cdot n_x} \quad B_{31} = \begin{pmatrix} 0 & . & . & 0 \\ \frac{k_{\mathrm{a}}\Delta t}{2} & 0 & . & . \\ 0 & . & 0 & . \\ 0 & 0 & \frac{k_{\mathrm{a}}\Delta t}{2} & 0 \end{pmatrix}_{n_x \cdot n_x}$$

$$B_{33} = \begin{pmatrix} 0 & . & . & 0 \\ 1 - \frac{\omega_{\mathrm{ML}} + k_{\mathrm{d}}\Delta t}{2} & 0 & . & . \\ 0 & . & 0 & . \\ 0 & 0 & 1 - \frac{\omega_{\mathrm{ML}} + k_{\mathrm{d}}\Delta t}{2} & 0 \end{pmatrix}_{n_x \cdot n_x}$$

$$B_{34} = \begin{pmatrix} 0 & . & . & 0 \\ \frac{\omega_{\mathrm{ML}} - k_{\mathrm{d}}\Delta t}{2} & 0 & . & . \\ 0 & . & 0 & . \\ 0 & 0 & \frac{\omega_{\mathrm{ML}} - k_{\mathrm{d}}\Delta t}{2} & 0 \end{pmatrix}_{n_x \cdot n_x}$$

$$G_1 = \begin{bmatrix} c_{\mathrm{M}}^0 \\ 0 \\ . \\ 0 \end{bmatrix}_{n_x}^{k+1} \quad G_2 = \begin{bmatrix} 0 \\ . \\ 0 \\ c_{\mathrm{M}}^* \end{bmatrix}_{n_x}^{k+1} \quad G_3 = \begin{bmatrix} 0 \\ . \\ . \\ 0 \end{bmatrix}_{n_x}^{k+1} \quad G_4 = \begin{bmatrix} 0 \\ . \\ 0 \\ c_{\mathrm{ML}}^* \end{bmatrix}_{n_x}^{k+1}$$

A.2.2 Diffusive scheme: matrices $A_{\mathbf{D}}$ and $B_{\mathbf{D}}$

Keeping the same notations as for the complete scheme, the only sub-matrices that change are:

$$B_{13} = B_{31} = 0$$

$$B_{11} = \begin{pmatrix} 0 & . & . & 0 \\ 1 - \frac{\omega_{\mathrm{M}}}{2} & 0 & . & . \\ 0 & . & 0 & . \\ 0 & 0 & 1 - \frac{\omega_{\mathrm{M}}}{2} & 0 \end{pmatrix}_{n_x \cdot n_x} \quad B_{12} = \begin{pmatrix} 0 & . & . & 0 \\ \frac{\omega_{\mathrm{M}}}{2} & 0 & . & . \\ 0 & . & 0 & . \\ 0 & 0 & \frac{\omega_{\mathrm{M}}}{2} & 0 \end{pmatrix}_{n_x \cdot n_x}$$

Published in Physical Chemistry Chemical Physics 2005, vol 7, p 3331-33-41
DOI: 10.1039/b505890b reprints also to galceran@quimica.udl.cat

$$B_{33} = \begin{pmatrix} 0 & . & . & 0 \\ 1-\frac{\omega_{\mathrm{ML}}}{2} & 0 & . & . \\ 0 & . & 0 & . \\ 0 & 0 & 1-\frac{\omega_{\mathrm{ML}}}{2} & 0 \end{pmatrix}_{n_x \cdot n_x} \qquad B_{34} = \begin{pmatrix} 0 & . & . & 0 \\ \frac{\omega_{\mathrm{ML}}}{2} & 0 & . & . \\ 0 & . & 0 & . \\ 0 & 0 & \frac{\omega_{\mathrm{ML}}}{2} & 0 \end{pmatrix}_{n_x \cdot n_x}$$

A.2.3 Reactive scheme: matrices $A_{\mathbf{R}}$ and $B_{\mathbf{R}}$

For the reactive scheme it is interesting to see the form of the matrices for the implicit scheme, because we are going to use the splitting only for fast chemical processes not convergent with the NS scheme. The new matrices take the following form:

$$A_{\mathrm{R}} = 1 + \begin{pmatrix} A'_{11} & A'_{12} & A'_{13} & A'_{13} \\ A'_{21} & A'_{22} & A'_{13} & A'_{13} \\ A'_{31} & A'_{31} & A'_{33} & A'_{34} \\ A'_{31} & A'_{31} & A'_{43} & A'_{44} \end{pmatrix}$$

$$A'_{11} = \tfrac{k_{\mathrm{a}}\Delta t}{2} \cdot diag(0,1,...,1)_{n_x \cdot n_x} \quad A'_{12} = diag(1, \tfrac{k_{\mathrm{a}}\Delta t}{2}, ..., \tfrac{k_{\mathrm{a}}\Delta t}{2})_{n_x \cdot n_x}$$

$$A'_{13} = -\tfrac{k_{\mathrm{d}}\Delta t}{2} \cdot diag(0,1,...,1)_{n_x \cdot n_x} \quad A'_{21} = diag(\tfrac{k_{\mathrm{a}}\Delta t}{2}, ..., \tfrac{k_{\mathrm{a}}\Delta t}{2}, 1)_{n_x \cdot n_x}$$

$$A'_{22} = \tfrac{k_{\mathrm{a}}\Delta t}{2} \cdot diag(1,...,1,0)_{n_x \cdot n_x} \quad A'_{31} = -\tfrac{k_{\mathrm{a}}\Delta t}{2} \cdot diag(0,1,...,1)_{n_x \cdot n_x}$$

$$A'_{33} = diag(1, \tfrac{k_{\mathrm{d}}\Delta t}{2}, ..., \tfrac{k_{\mathrm{d}}\Delta t}{2})_{n_x \cdot n_x} \quad A'_{34} = diag(-1, \tfrac{k_{\mathrm{d}}\Delta t}{2}, ..., \tfrac{k_{\mathrm{d}}\Delta t}{2})_{n_x \cdot n_x}$$

$$A'_{43} = diag(\tfrac{k_{\mathrm{d}}\Delta t}{2}, ..., \tfrac{k_{\mathrm{d}}\Delta t}{2}, 1)_{n_x \cdot n_x} \quad A'_{44} = \tfrac{k_{\mathrm{d}}\Delta t}{2} \cdot diag(1,...,1,0)_{n_x \cdot n_x}$$

$$B_{\mathrm{R}} = diag(0,1,...,1,0,0,1,...,1,0)_{16 \cdot n_x^2}$$

A.3 Numerical errors

In general, the numerical scheme, whatever methods we have chosen, takes the following form:

$$Au^{n+1} = Bu^n + G \tag{60}$$

where u^n is the vector of the density distribution functions, discretized in space and time, n is the time step level $t_n = n\Delta t$, G is a vector taking into account the boundary conditions and possibly, the non linearity of the problem, A and B are operators depending on the boundary conditions and specifically on the numerical method of integration. For instance, considering the particular problem introduced in appendix A.2, for the NS scheme A and B take the form defined in sub-appendix A.2.1, for the D process $A = A_{\mathrm{D}}$ and $B = B_{\mathrm{D}}$ (see sub-appendix A.2.2) and for the R process $A = A_{\mathrm{R}}$ and $B = B_{\mathrm{R}}$ (see sub-appendix A.2.3).

Published in Physical Chemistry Chemical Physics 2005, vol 7, p 3331-33-41
DOI: 10.1039/b505890b reprints also to galceran@quimica.udl.cat

When G does not contain any non linearity, the scheme (60) is convergent if the spectral radius of iteration matrix $A^{-1}B$ is less than one [19]:

$$\rho(A^{-1}B) < 1 \tag{61}$$

for $t \in [n\Delta t, (n+1)\Delta t]$. We will use inequality (61) to study the convergence conditions of the different schemes.
We consider only complexes for which $K' > 1$. The complete linear scheme, i.e. the case of excess of ligand solved with the complete scheme (20) gives the following convergence condition:

$$\Delta t < \frac{2}{k_{\mathrm{a}} c^*_{\mathrm{L}}} \tag{62}$$

Indeed, the spectral radius of the iteration matrix is equal to the maximum value of all its eigenvalues and one of the important properties is that $\rho(A^{-1}B) \leq \|A^{-1}B\|$. Then the proof of condition (62) reduces to study the norm $\|A^{-1}B\|$. Considering the explicit form of the matrices A and B given in sub-appendix A.2.1, we have $\|A\| \leq 2$, so $1/\|A^{-1}\| \leq \|A\| \leq 2$, and $\|B\| \leq k'_{\mathrm{a}}\Delta t$. Therefore, $\|A^{-1}B\| \leq \|A^{-1}\|\|B\| \leq \|A^{-1}\|k'_{\mathrm{a}}\Delta t$ and by applying the convergent condition (61) we get inequality (62).
The application of the splitting time procedure to the same problem is possible numerically for any values of k_{a}, because inequality (61) is always satisfied. So the complete scheme is conditionally convergent while the split scheme is always convergent.
The convergence of the non linear scheme has to be investigated by applying the fixed point theorem [19], also known as the Banach theorem. Roughly speaking, the theorem says that a numerical scheme $u^{n+1} = Tu^n$, where T is a (non linear) operator, is convergent to a unique solution if T is a contraction, i.e.

$$\forall u, v \quad \exists 0 \leq L < 1 \text{ such that} \quad \|Tu - Tv\| \leq L\|u - v\| \tag{63}$$

By using the Banach theorem to the reactive part of the time split procedure solved with the implicit Euler method, equation (35), we obtain that the numerical scheme is always convergent. Indeed, the numerical reactive scheme takes the form $u^{n+1} = u^n + Fu^{n+1}$, where F is a non linear operator, and it can be put in the form $u^{n+1} = Tu^n$, where $T = \bar{F}^{-1}$ and $\bar{F}u = u - Fu$. Therefore, $\|Tu - Tv\| \leq \|(1-F)^{-1}\|\|u - v\|$, and, because of $\|(1-F)^{-1}\| < 1$ for each F, the Banach theorem holds.

B List of symbols

In the following tables we show the list of the symbols encountered in the paper.

Published in Physical Chemistry Chemical Physics 2005, vol 7, p 3331-33-41
DOI: 10.1039/b505890b reprints also to galceran@quimica.udl.cat

SYMBOL	MEANING	EQUATION
δ_{X}	Diffusion layer thickness of species X	(2)
Δx	space mesh grid size	(20)
Δt	time mesh grid size	(20)
Δt_{D}	Diffusion time scale	(33)
Δt_{K}	Reaction time scale	(29)
ϵ_r	Relative error (for the flux)	(49)
μ	Reaction layer thickness	(3)
$\Omega^{\mathrm{NR}}_{f_{i,\mathrm{X}}}$	Non-reactive operator	(21)
$\Omega^{\mathrm{R}}_{f_{i,\mathrm{X}}}$	Reactive operator	(22)
ω_{X}	Relaxation parameter of the LBGK diffusive scheme	(23)

Greek symbols appearing in the paper.

Published in Physical Chemistry Chemical Physics 2005, vol 7, p 3331-33-41
DOI: 10.1039/b505890b reprints also to galceran@quimica.udl.cat

SYMBOL	MEANING	EQUATION
A, B, G	Matrices and vector of a general numerical scheme	(60)
A_{D}, B_{D}	Matrices of the diffusion process D	(A.2.2)
A_{R}, B_{R}	Matrices of the reaction process R	(A.2.3)
c_{X}	Concentration of the species X	(4)
c^*_{X}	Bulk value of species X	(10)
$c^*_{\mathrm{X,tot}}$	Total bulk concentration of species X	(9)
d	Dimension of cubic-like lattice	(19)
D_{X}	Diffusion coefficient of X species	(4)
$\bar{D}_{\mathrm{M}}$	Average diffusion coefficient	(48)
$f_{i,\mathrm{X}}$	Density distribution function of species X having discrete velocity v_i	(19)
$f^{eq}_{i,\mathrm{X}}$	Equilibrium density distribution function	(24)
$\bar{f}_{i,\mathrm{X}}$	Pseudo-density distribution function (for diffusion process)	(33)
$\tilde{f}_{i,\mathrm{X}}$	Pseudo-density distribution function (for reactive process)	(34)
J_{inert}	Analytical solution of the flux in the totally inert case	(47)
J_{labile}	Analytical solution of the flux in the fully labile case	(48)
J_{M}	Flux of M crossing the electrode surface	(28)
$J_{\mathrm{M,tot,\ no\ ligand}}$	Flux of total M at the electrode surface, with no ligand	(51)
K	Equilibrium constant	(9)
k_{a},k_{d}	Association and dissociation rate constants	(1)
$k^{(i)}_{\mathrm{d}}$,$k^{(i)}_{\mathrm{a}}$	Dissociation and association rate constants for reaction $\mathrm{M} + \mathrm{L}_i \rightleftharpoons \mathrm{ML}_i$	(54)
L	Ligand	(1)
L_h	Ligand species h	(54)
M	Metal ion	(1)
M^0	Metal reduced form	(1)
ML	Complex	(1)
n	Number of electrons involved in the electrode reduction	(1)
n_x	Number of discretization points in space domain	(20)
n_t	Total number of time-step iterations	(20)
n^{tot}_{D}	Number of iterations during D process	(33)
n^{tot}_{K}	Number of iterations during R process	(34)
R	Reactive term	(8)
T_{D}	Diffusion operator	(57)
T_{R}	Reaction operator	(57)
$u(x,t)$	Analytical solution for the concentration profile of M	(45)
v_i	Lattice velocity along i-direction	(18)
(x_j, t_n)	Point in the space-time grid	(20)
z	Coordination number	(16)

Latin symbols appearing in the paper.

Published in Physical Chemistry Chemical Physics 2005, vol 7, p 3331-33-41
DOI: 10.1039/b505890b reprints also to galceran@quimica.udl.cat

References

[1] J. Buffle and G. Horvai (Eds), In situ monitoring of aquatic systems, Vol.6 in IUPAC Series on Analytical and Physical Chemistry of Environmental Systems (J.Buffle, H.Leeuwen series Eds), John Wiley and Sons Inc., 2000.

[2] J. Galceran, J. Puy, J. Salvador, J. Cecilia, F. Mas and J.L. Garces, *Phys. Chem. Chem. Phys.,* 2003, **5**(22), 5091.

[3] D.A. Wolf-Gladrow, Lattice Gas Cellular Automata and Lattice Boltzman Models: An introduction, Printed in Berlin, Springer-Verlag, 2000.

[4] W. Hundsdorfer and J.G. Verwer, Numerical Solution of Time-Dependent Advection-Diffusion-Reaction Equations, Printed in Berlin, Springer-Verlag, 2003.

[5] http://www.epsilon-web.net/Ec/digisim/bibdig.html: A list of algorithm for digital simulation in electrochemistry

[6] D. Britz, Digital Simulation in Electrochemistry, Printed in Berlin, Springer, 1988.

[7] J. Galceran, D.J. Gavaghan and J.S. Rollett, *Journal of Electroanalytical Chemistry*, 1995, **394**, 17.

[8] J. Puy, J. Galceran, J. Salvador, J. Cecilia, J.M. Diaz-Cruz, M. Esteban and F. Mas, *Journal of Electroanalytical Chemistry*, 1994, **374**, 223.

[9] F.L. Qiu, and A.C. Fisher, *Electrochemistry Communications*, 2001, **3**(3), 117.

[10] B. Chopard and M. Droz, Cellular Automata Modelling of Physical Systems, Cambridge Univ. Press. UK, 1988

[11] S. Dawson, S. Chen and G.D. Doolen, *Journal of Chemical Physics*, 1992, **98**, 1514.

[12] Q. Li, C. Zheng, N. Wang and B. Shi, *Journal of Scientific Computing*, 2001, **16**(2), 121.

[13] N. Yanenko, Methodes a pas fractionnaire, Librairie Armand Colin, (Paris), 1968.

[14] D. Ropp, J. Shadid and C. Ober, *Journal of Computational Physics*, 2004, **194**(2), 544.

[15] B. Chopard and P. Luthi, *Physical Reviews Letters,* 1994, **72**(9), 1384.

[16] P. Albuquerque, D. Alemani, B. Chopard and P. Leone, *Computational Science - ICCS 2004: 4th International Conference*, 2004, **3039**, 540.

Published in Physical Chemistry Chemical Physics 2005, vol 7, p 3331-33-41
DOI: 10.1039/b505890b reprints also to galceran@quimica.udl.cat

[17] H. Leeuwen, J. Puy, J. Galceran and J. Cecilia, *Journal of Electroanalytical Chemistry*, 2002, **526**, 10.

[18] S. Succi, *The Lattice Boltzmann Equation*, 2001, Oxford Science Publication.

[19] V. Comincioli, *Analisi Numerica*, 1995, Printed in Milano, Mc-Graw Hill.

[20] H. De Jong and H. Leeuwen, *Journal of Electroanalytical Chemistry*, 1987, **234**, 1.

[21] J. Heyrowsky and J. Kuta, *Principles of Polarography*, 1966, Academic Press.

[22] X. He and L-S Luo, *Physical Review E*, 1997, **56**, 6811.

[23] P.L. Bhatnagar, E.P. Gross and M. Krook, *Physical Review*, 1954, **94**, 511.

[24] A.J. Bard and L.R. Faulkner, *Electrochemical Methods: Fundamentals and Applications*, 1980, J. Wiley NY.

[25] Hollenbeck, K.J. (1998) INVLAP.M: A matlab function for numerical inversion of Laplace transforms by the De Hoog algorithm, http://www.isva.dtu.dk/staff/karl/invlap.htm.

Published in Physical Chemistry Chemical Physics 2005, vol 7, p 3331-33-41
DOI: 10.1039/b505890b reprints also to galceran@quimica.udl.cat

Table 1: Relative computational costs normalised with respect to the explicit RD scheme. RD explicit simulations takes around 4 seconds on a Pentium 4 to perform 1000 iteration steps in a lattice with 1000 points.

	RD	DR	DRD	RDR
Explicit	1	1	1.1	1.8
Implicit	5.3	5.3	5.4	10.4

Table 2: Relative error, eq. (49), for flux computation in the inert case for different Δt values. Parameters' values are: $K' = Kc^*_{\mathrm{L}} = 100$, $D_{\mathrm{M}} = D_{\mathrm{ML}} = D_{\mathrm{L}} = 10^{-10} m^2/s$, $k_{\mathrm{a}} = 10^{-10} \frac{m^3}{mol \cdot s}$, $\Delta x = 2\mu m$, $t = 0.2s$, $c^*_{\mathrm{M,tot}} = 10^{-3} mol/m^3$, $c^*_{\mathrm{L}} = 1 mol/m^3$.

Δt	ϵ_r
10^{-2}	0.32%
10^{-3}	0.25%
10^{-4}	0.25%

Table 3: Relative error, eq. (50) for flux computation in the fully labile linear (excess of ligand) case for different Δt values, computed with the RD scheme. Parameters' values are: $K' = Kc^*_{\mathrm{L}} = 100$, $D_{\mathrm{M}} = D_{\mathrm{ML}} = D_{\mathrm{L}} = 10^{-10} m^2/s$, $k_{\mathrm{a}} = 10^{10} \frac{m^3}{mol \cdot s}$, $\Delta x = 2\mu m$, $t = 0.1s$, $c^*_{\mathrm{M,tot}} = 10^{-3} mol/m^3$, $c^*_{\mathrm{L}} = 1 mol/m^3$.

Δt	ϵ_r
10^{-2}	3.79%
10^{-3}	2.90%
10^{-4}	2.88%

Published in Physical Chemistry Chemical Physics 2005, vol 7, p 3331-33-41
DOI: 10.1039/b505890b reprints also to galceran@quimica.udl.cat

Table 4: Normalised flux results of numerical simulations for several values of k_{d} with the following parameters: $K' = Kc^*_{\mathrm{L}} = 10$, $D_{\mathrm{M}} = D_{\mathrm{ML}} = 10^{-9}m^2/s$, $t = 0.01s$, $\Delta x = 0.1\mu m$, $\Delta t = 10\mu s$, $\Delta t_{\mathrm{R}} = 0.2\mu s$, $c_{\mathrm{M,tot}} = 10^{-3}mol/m^3$, $c^*_{\mathrm{L}} = 1mol/m^3$, $n_x = 201$.

$k_{\mathrm{d}}(s^{-1})$	Φ RD	Φ NS	Φ Numerical Laplace inversion
10^{-3}	0.09094	0.09099	0.09092
10^{-2}	0.09103	0.09107	0.09100
10^{-1}	0.09184	0.09189	0.09182
1	0.09983	0.09987	0.09981
10	0.16578	0.16578	0.16578
10^2	0.41472	0.41429	0.41496
10^3	0.76372	0.76263	0.76977
10^4	0.92308	0.92070	0.95962
10^5	0.93563	not convergent	0.99551
10^6	0.93563	not convergent	0.99955
10^7	0.93563	not convergent	0.99995

Table 5: Normalised flux results of numerical simulations with the following parameters: $K' = Kc^*_{\mathrm{L}} = 10$, $D_{\mathrm{M}} = D_{\mathrm{ML}} = 10^{-9}m^2/s$, $t = 0.5s$, $\Delta x = 1\mu m$, $\Delta t = 0.1ms$, $\Delta t_{\mathrm{R}} = 50\mu s$, $c_{\mathrm{M,tot}} = 10^{-3}mol/m^3$, $c^*_{\mathrm{L}} = 1mol/m^3$, $n_x = 201$.

$k_{\mathrm{d}}(s^{-1})$	Φ RD	Φ NS	Φ Numerical Laplace inversion
10^{-5}	0.09096	0.09093	0.09091
10^{-4}	0.09101	0.09098	0.09095
10^{-3}	0.09141	0.09138	0.09136
10^{-2}	0.09545	0.09543	0.09541
10^{-1}	0.13196	0.13195	0.13194
1	0.31929	0.31949	0.31954
10	0.66661	0.66792	0.66867
10^2	0.91865	0.92330	0.92660
10^3	0.98150	0.98113	0.99114
10^4	0.98828	not convergent	0.99909
10^5	0.98828	not convergent	0.99991

Published in Physical Chemistry Chemical Physics 2005, vol 7, p 3331-33-41
DOI: 10.1039/b505890b reprints also to galceran@quimica.udl.cat

Fig. 1 Schematic representation of the physicochemical problem. The metal ion M can form a complex ML with a ligand L, having an association rate constant k_a and a dissociation rate constant k_d. Each of the three species diffuse in solution. M can also be reduced at the electrode surface into M^0 through a reversible process. Also the diffusion layer, δ, and the reaction layer thickness μ are shown in the picture: the diffusion layer is the region in the vicinity of an electrode where the concentration is significantly different from the bulk value; within the reaction layer, any M dissociated from ML can be either recombined to L as ML or reduced into M^0 at the electrode surface.

Fig. 2 Example of RD, DR and DRD splittings. (See text for details).

Fig. 3 Error in the L_2-norm, eq. (46), on the concentration profile vs the number of iteration steps. The diffusion coefficients are all equal to $10^{-9}m^2/s$, $K' = Kc_L^* = 0.1$, $k_d = 10^{-7}s^{-1}$, $k_a = 10^{-8}$, $mol/m^3 s$ $t = 1ms$, $\Delta x = 10^{-6}m$, $n_x = 201$, $c^*_{M,tot} = 10^{-3}mol/m^3$, $c_L^* = 1mol/m^3$. A reference slope of -1 has been added to compare the numerical scheme. The splittings are solved using the same integration time steps for the diffusion and the reaction schemes. Nodes NS and RD on one hand and DR and RDR on the other hand are indistinguishable in the plot, because they give almost the same errors.

Fig. 4 Relative error on the flux, computed from expression (53), at $t = 0.1s$ computed for several equilibrium constants as a function of the ratio $\frac{\Delta t}{\Delta x}$, in excess of ligand condition. All the diffusion coefficients are the same ($D_x = 10^{-9}m^2/s$). Number of iteration steps are 1000 in all the simulations. $c_L^* = 1mol/m^3$, $k_d = 1s^{-1}$. Plot A: $K = 10m^3/mol$, plot B: $K = 100m^3/mol$, plot C: $K = 1000m^3/mol$, plot D: $K = 10000m^3/mol$. Same markers as in figure 3. The RD scheme, compared with the others splitting schemes, seems to be the best splitting scheme, in all cases.

Fig. 5 Plot of the error on the flux after 1000 time step iterations as function of $K' = Kc_L^* = k_a/k_d c_L^*$ and of the ratio $\frac{\Delta x}{\mu}$. Computation with RD scheme. $k_d = 100s^{-1}$, same diffusion coefficients for all species $D_x = 10^{-10}m^2/s$. We see that for significant contribution of the complex (i.e. when $K' > 1$), the error is negligible (less than 1%) only for $\Delta x < \mu$.

Fig. 6 Flux at the planar electrode surface for an intermediate kinetic case computed with RD scheme: for short times the system behaves as inert ($\mu < \delta$), but at long times the system is labile ($\mu > \delta$) due the increase of δ with time. Solid line (-): equation (48), dashed-dotted line (-.): equation (47), crossed line (+): numerical results. Parameters:$\Delta x = 1\mu m$, $\Delta t = 0.25ms$, $D_M = D_{ML} = D_L = 10^{-9}m^2/s$,

Published in Physical Chemistry Chemical Physics 2005, vol 7, p 3331-33-41
DOI: 10.1039/b505890b reprints also to galceran@quimica.udl.cat

$k_a = 1000 m^3/mol \cdot s$, $k_d = 10 s^{-1}$, $K' = K c^*_L = 1$, $c^*_M = 5 \cdot 10^{-4} mol/m^3$, $c^*_{ML} = 5 \cdot 10^{-4} mol/m^3$, $c^*_L = 1 mol/m^3$.

Fig. 7 Comparison of the flux computed by numerical inversion of the analytical flux solution, equation (52) (circles) and by numerical simulation obtained by NS scheme (20) (dashed-dotted line) and RD scheme (dashed line) for 100 seconds of electrolysis. $\Delta x = 50 \mu m$, $\Delta t = 0.1 ms$, $D_M = 10^{-7} m^2/s$, $D_L = D_{ML} = 10^{-11} m^2/s$, $k_a = 10 m^3/mol \cdot s$, $K = 10 m^3/mol$, $c^*_L = 1 mol/m^3$. The circle values (o) are taken from table 2 (column a) of [20].

Fig. 8 Two complexes, ML_1 and ML_2 with ligand excess. Parameters: $D_X = 10^{-10} m^2/s$ for all the species, $k_a^{(1)} = 10^4 mol^{-1} m^3 s^{-1}$, $k_d^{(1)} = 10^3 s^{-1}$, $k_a^{(2)} = 10^{-2} mol^{-1} m^3 s^{-1}$, $k_d^{(2)} = 10^{-3} s^{-1}$, $c^*_{M,tot} = 10^{-3} mol/m^3$, $c^*_{L_1} = c^*_{L_2} = 1 mol/m^3$, $c^*_{ML_1} = c^*_{ML_2} = 4.76 \cdot 10^{-4} mol/m^3$, $\Delta t = 10^{-5} s$, $\Delta x = 0.05 \mu m$, $n_x = 1000$. The plot shows the flux computed from equation (28) (dashed line –) obtained by the numerical simulation with the RD scheme. It is compared with the fluxes under in the fully inert (solid line) and labile (dashed-dotted line -.) conditions, eq. (47) and (48) respectively, with $\bar{D}_M = \frac{D_M c^*_M + D_{ML_1} c^*_{ML_1} + D_{ML_2} c^*_{ML_2}}{c^*_M + c^*_{ML_1} + c^*_{ML_2}}$.

Fig. 9 Two complexes, ML_1 and ML_2 with ligand excess. Concentration profiles of M and ML_1 as a function of the distance x from the electrode surface. The concentration ratio depicted in the inset is defined as c_X/c^*_X for X=M and ML_1. Other parameters are as in figure 8. The reaction layer thickness for the reaction $M + L_1 \rightleftharpoons ML_1$ is $\mu_1 = 0.1 \mu m$. The profile concentrations of L_1, L_2 and ML_2 are not shown because they are constant due to the excess of L_1 and L_2 and the very low dynamics of ML_2.

Fig. 10 One complex, ML, without excess of ligand. Flux of metal M at $x = 0$ by using the RD scheme, in the following conditions: $K = 100 m^3/mol$, $k_a = 10^4 m^3/mol \cdot s$, $D_M = D_L = D_{ML} = 10^{-10} m^2/s$, $c^*_{M,tot} = 0.02 mol/m^3$, $c^*_L = 0.02 mol/m^3$, $\Delta t = 0.01 ms$, $\omega_M = \omega_L = \omega_{ML} = 1.98$, $\Delta x = 0.18 \mu m$. The analytical solution for the flux in the labile case, shown for comparison, is valid only in presence of excess of ligand. Dashed-dotted line (-.): labile complex, eq. (48); solid line (-): inert complex, eq. (47); dashed line (–): numerical solution.

Fig. 11 Two complexes, ML_1 and ML_2, without ligand excess. Parameters: $D = 10^{-10} m^2/s$ for all the species, $k_a^{(1)} = 10^6 mol^{-1} m^3 s^{-1}$, $k_d^{(1)} = 10^2 s^{-1}$, $k_a^{(2)} = 10^{-2} mol^{-1} m^3 s^{-1}$, $k_d^{(2)} = 10^{-6} s^{-1}$, $c^*_{M,tot} = 10^{-3} mol/m^3$, $c^*_{L_1} = c^*_{L_2} = 5 \cdot 10^{-4} mol/m^3$, $c^*_{ML_1} = c^*_{ML_2} = 4.55 \cdot 10^{-4} mol/m^3$, $\Delta t = 10^{-3} s$, $\Delta x = 0.3 \mu m$, $n_x = 300$. The plot shows the flux computed with equation (28) (dashed line (–)) obtained by the numerical simulation

Published in Physical Chemistry Chemical Physics 2005, vol 7, p 3331-33-41
DOI: 10.1039/b505890b reprints also to galceran@quimica.udl.cat

of the RD scheme compared with the flux in the fully inert (solid line (-)) and labile (dashed-dotted (-.)) complexes in excess of ligands, eqns. (47) and (48) respectively.

Fig. 12 Two complexes, ML_1 and ML_2, without ligand excess. Normalised concentration profiles of M, ML_1 and L_1, as a function of the distance from the electrode. Other parameters as in figure 11. The reaction layer thickness for the reaction $M + L_1 \rightleftharpoons ML_1$ is $\mu_1 = 0.45\mu m$. The normalised concentration profiles of L_2 and ML_2 are not shown because they are horizontal and equal to 1.0, due to the very low dynamics of ML_2.

Fig. 13 One complex ML in non excess of ligand. Normalised concentration profiles corresponding to $k_a = 10^8 mol^{-1}m^3s^{-1}$, $k_d = 500s^{-1}$,$\mu = 0.7\mu m$, $c^*_{M,tot} = 0.1mol \cdot m^{-3}$, $c^*_{L,tot} = 0.08mol \cdot m^{-3}$, $t = 1s$, $D_M = 10^{-9}m^2/s$, $D_{ML} = D_L = 10^{-10}m^2/s$, $\Delta t = 10^{-4}s$, $\Delta x = \mu$. Profiles of M, ML and L correspond to the ratios c_M/c^*_M, c_{ML}/c^*_{ML} and $c_L/c_L(0)$, respectively. Continuous lines are obtained by numerical simulations using the RD scheme. Circles (o) and crosses (+) correspond to the values of L and ML shown in figure 7 of [17].

Fig. 14 Memorandum of the application of the numerical schemes proposed. The LBGK scheme, equation (20), is convergent only under a time condition $\Delta t < 2/k_a c_L$, while by using the splitting scheme RD the convergence is ensured for any time step Δt. On the other hand, both NS and RD schemes need a grid refinement near the electrode, because Δx must be less than the reaction layer thickness μ, which is inversely proportional to $k_a^{1/2}$.

Published in Physical Chemistry Chemical Physics 2005, vol 7, p 3331-33-41
DOI: 10.1039/b505890b reprints also to galceran@quimica.udl.cat

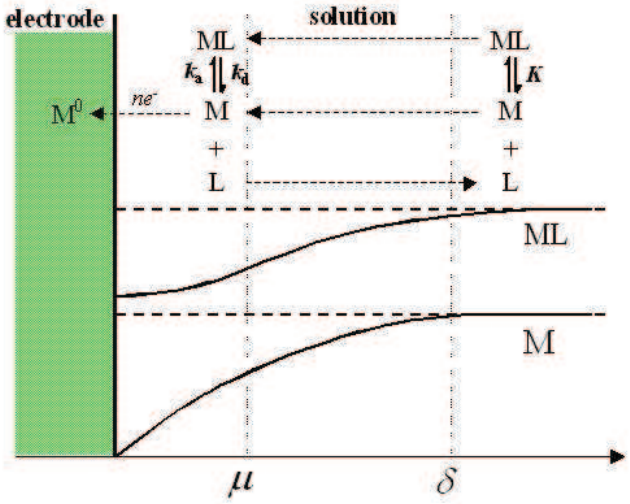

Figure 1: Schematic representation of the physicochemical problem. The metal ion M can form a complex ML with a ligand L, having an association rate constant k_a and a dissociation rate constant k_d. Each of the three species diffuse in solution. M can also be reduced at the electrode surface into M^0 through a reversible process. Also the diffusion layer, δ, and the reaction layer thickness μ are shown in the picture: the diffusion layer is the region in the vicinity of an electrode where the concentration is significantly different from the bulk value; within the reaction layer, any M dissociated from ML can be either recombined to L as ML or reduced into M^0 at the electrode surface.

Published in Physical Chemistry Chemical Physics 2005, vol 7, p 3331-33-41
DOI: 10.1039/b505890b reprints also to galceran@quimica.udl.cat

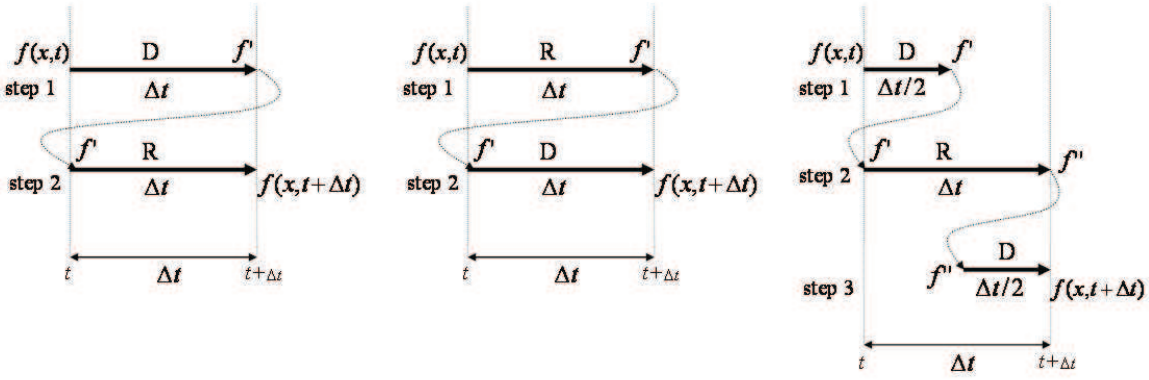

Figure 2: Example of RD, DR and DRD splittings. (See text for details).

Published in Physical Chemistry Chemical Physics 2005, vol 7, p 3331-33-41
DOI: 10.1039/b505890b reprints also to galceran@quimica.udl.cat

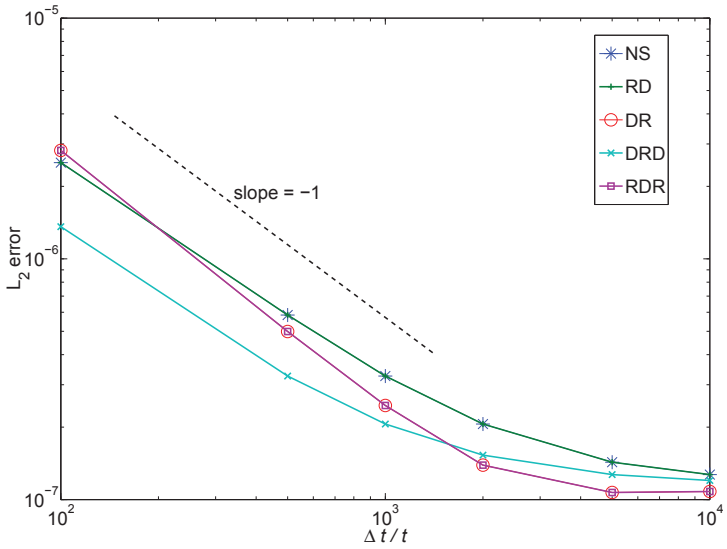

Figure 3: Error in the L_2-norm, eq. (46), on the concentration profile vs the number of iteration steps. The diffusion coefficients are all equal to $10^{-9}m^2/s$, $K' = Kc^*_{\mathrm{L}} = 0.1$, $k_{\mathrm{d}} = 10^{-7}s^{-1}$, $k_{\mathrm{a}} = 10^{-8}$, $mol/m^3 s$ $t = 1ms$, $\Delta x = 10^{-6}m$, $n_x = 201$, $c^*_{\mathrm{M,tot}} = 10^{-3}mol/m^3$, $c^*_{\mathrm{L}} = 1mol/m^3$. A reference slope of -1 has been added to compare the numerical scheme. The splittings are solved using the same integration time steps for the diffusion and the reaction schemes. Nodes NS and RD on one hand and DR and RDR on the other hand are indistinguishable in the plot, because they give almost the same errors.

Published in Physical Chemistry Chemical Physics 2005, vol 7, p 3331-33-41
DOI: 10.1039/b505890b reprints also to galceran@quimica.udl.cat

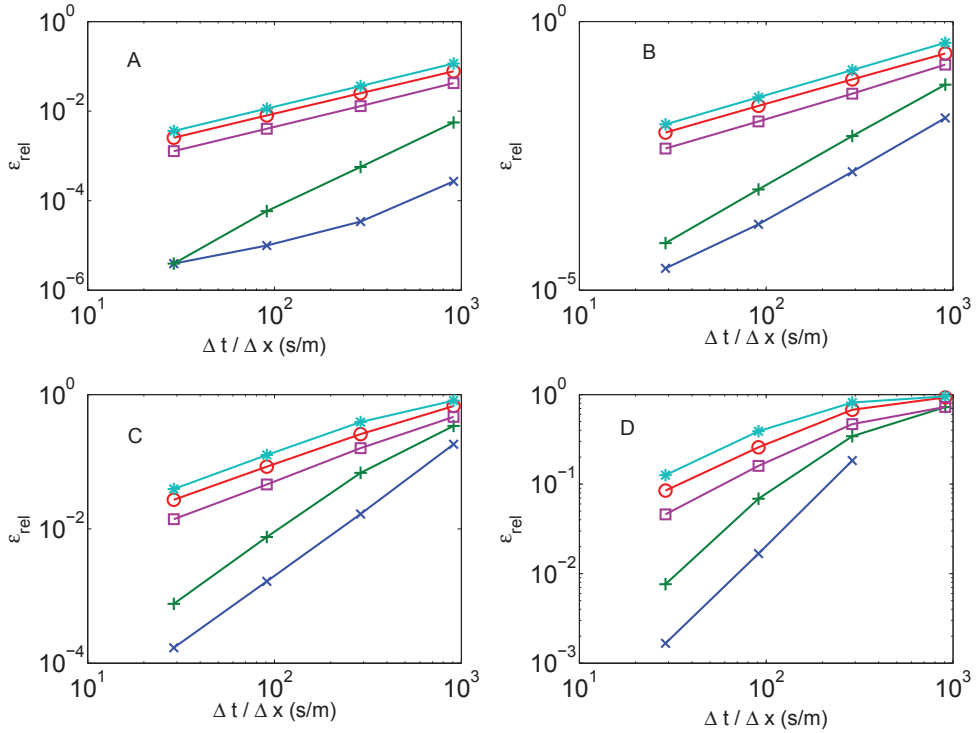

Figure 4: Relative error on the flux, computed from expression (53), at $t = 0.1s$ computed for several equilibrium constants as a function of the ratio $\frac{\Delta t}{\Delta x}$, in excess of ligand condition. All the diffusion coefficients are the same ($D_{\mathrm{x}} = 10^{-9} m^2/s$). Number of iteration steps are 1000 in all the simulations. $c^*_{\mathrm{L}} = 1 mol/m^3$, $k_{\mathrm{d}} = 1 s^{-1}$. Plot A: $K = 10 m^3/mol$, plot B: $K = 100 m^3/mol$, plot C: $K = 1000 m^3/mol$, plot D: $K = 10000 m^3/mol$. Same markers as in figure 3. The RD scheme, compared with the others splitting schemes, seems to be the best splitting scheme, in all cases.

Published in Physical Chemistry Chemical Physics 2005, vol 7, p 3331-33-41
DOI: 10.1039/b505890b reprints also to galceran@quimica.udl.cat

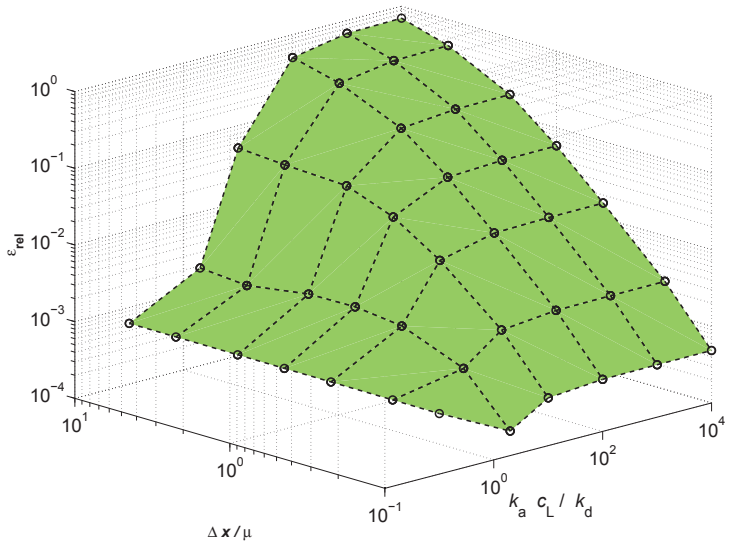

Figure 5: Plot of the error on the flux after 1000 time step iterations as function of $K' = Kc_{\mathrm{L}}^* = k_{\mathrm{a}}/k_{\mathrm{d}}c_{\mathrm{L}}^*$ and of the ratio $\frac{\Delta x}{\mu}$. Computation with RD scheme. $k_{\mathrm{d}} = 100s^{-1}$, same diffusion coefficients for all species $D_{\mathrm{x}} = 10^{-10}m^2/s$. We see that for significant contribution of the complex (i.e. when $K' > 1$), the error is negligible (less than 1%) only for $\Delta x < \mu$.

Published in Physical Chemistry Chemical Physics 2005, vol 7, p 3331-33-41
DOI: 10.1039/b505890b reprints also to galceran@quimica.udl.cat

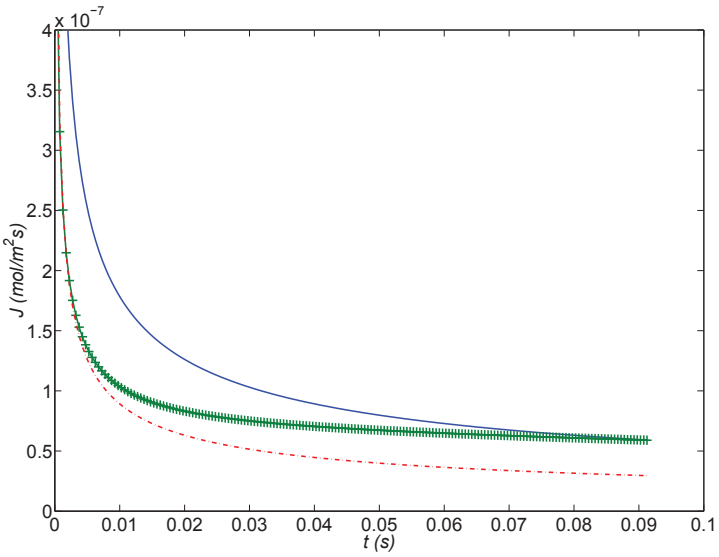

Figure 6: Flux at the planar electrode surface for an intermediate kinetic case computed with RD scheme: for short times the system behaves as inert ($\mu < \delta$), but at long times the system is labile ($\mu > \delta$) due the increase of δ with time. Solid line (-): equation (48), dashed-dotted line (-.): equation (47), crossed line (+): numerical results. Parameters:$\Delta x = 1\mu m$, $\Delta t = 0.25ms$, $D_{\mathrm{M}} = D_{\mathrm{ML}} = D_{\mathrm{L}} = 10^{-9}m^2/s$, $k_{\mathrm{a}} = 1000m^3/mol \cdot s$, $k_{\mathrm{d}} = 10s^{-1}$, $K' = Kc^*_{\mathrm{L}} = 1$, $c^*_{\mathrm{M}} = 5 \cdot 10^{-4}mol/m^3$, $c^*_{\mathrm{ML}} = 5 \cdot 10^{-4}mol/m^3$, $c^*_{\mathrm{L}} = 1mol/m^3$

Published in Physical Chemistry Chemical Physics 2005, vol 7, p 3331-33-41
DOI: 10.1039/b505890b reprints also to galceran@quimica.udl.cat

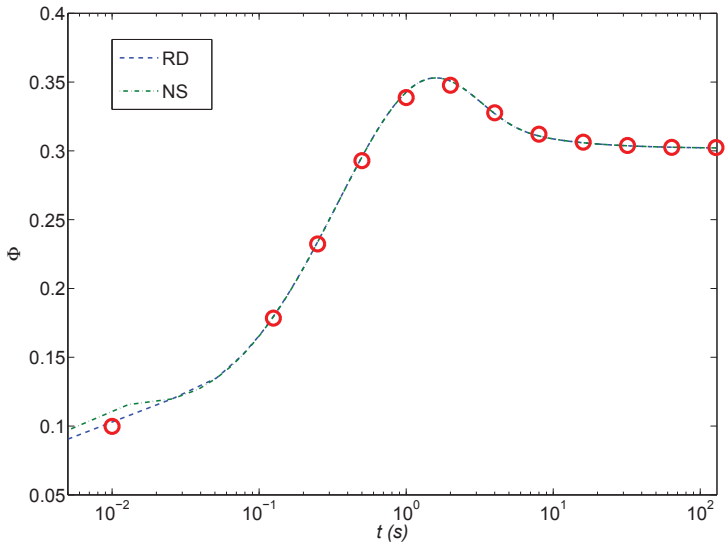

Figure 7: Comparison of the flux computed by numerical inversion of the analytical flux solution, equation (52) (circles) and by numerical simulation obtained by NS scheme (20) (dashed-dotted line) and RD scheme (dashed line) for 100 seconds of electrolysis. $\Delta x = 50\mu m$, $\Delta t = 0.1ms$, $D_{\mathrm{M}} = 10^{-7}m^2/s$, $D_{\mathrm{L}} = D_{\mathrm{ML}} = 10^{-11}m^2/s$, $k_{\mathrm{a}} = 10m^3/mol \cdot s$, $K = 10m^3/mol$, $c_{\mathrm{L}}^* = 1mol/m^3$. The circle values (o) are taken from table 2 (column a) of [20].

Published in Physical Chemistry Chemical Physics 2005, vol 7, p 3331-33-41
DOI: 10.1039/b505890b reprints also to galceran@quimica.udl.cat

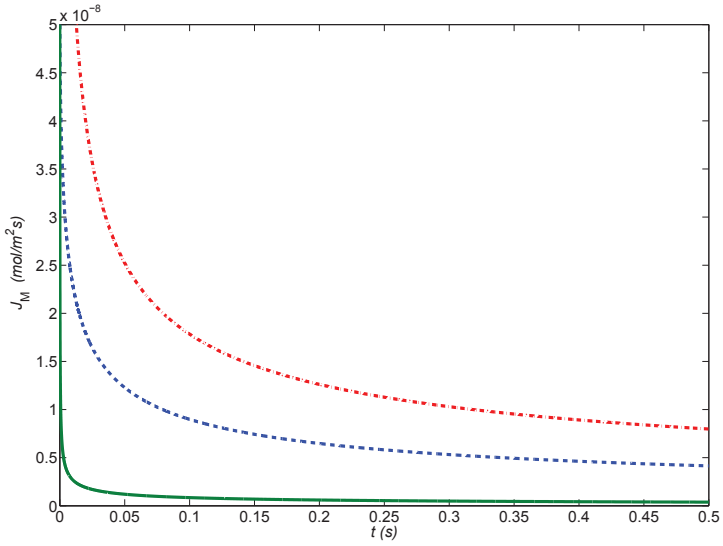

Figure 8: Two complexes, ML_1 and ML_2 with ligand excess. Parameters: $D_X = 10^{-10} m^2/s$ for all the species, $k_a^{(1)} = 10^4 mol^{-1} m^3 s^{-1}$, $k_d^{(1)} = 10^3 s^{-1}$, $k_a^{(2)} = 10^{-2} mol^{-1} m^3 s^{-1}$, $k_d^{(2)} = 10^{-3} s^{-1}$, $c^*_{M,tot} = 10^{-3} mol/m^3$, $c^*_{L_1} = c^*_{L_2} = 1 mol/m^3$, $c^*_{ML_1} = c^*_{ML_2} = 4.76 \cdot 10^{-4} mol/m^3$, $\Delta t = 10^{-5} s$, $\Delta x = 0.05 \mu m$, $n_x = 1000$. The plot shows the flux computed from equation (28) (dashed line –) obtained by the numerical simulation with the RD scheme. It is compared with the fluxes under in the fully inert (solid line) and labile (dashed-dotted line -.) conditions, eq. (47) and (48) respectively, with $\bar{D}_M = \frac{D_M c^*_M + D_{ML_1} c^*_{ML_1} + D_{ML_2} c^*_{ML_2}}{c^*_M + c^*_{ML_1} + c^*_{ML_2}}$.

Published in Physical Chemistry Chemical Physics 2005, vol 7, p 3331-33-41
DOI: 10.1039/b505890b reprints also to galceran@quimica.udl.cat

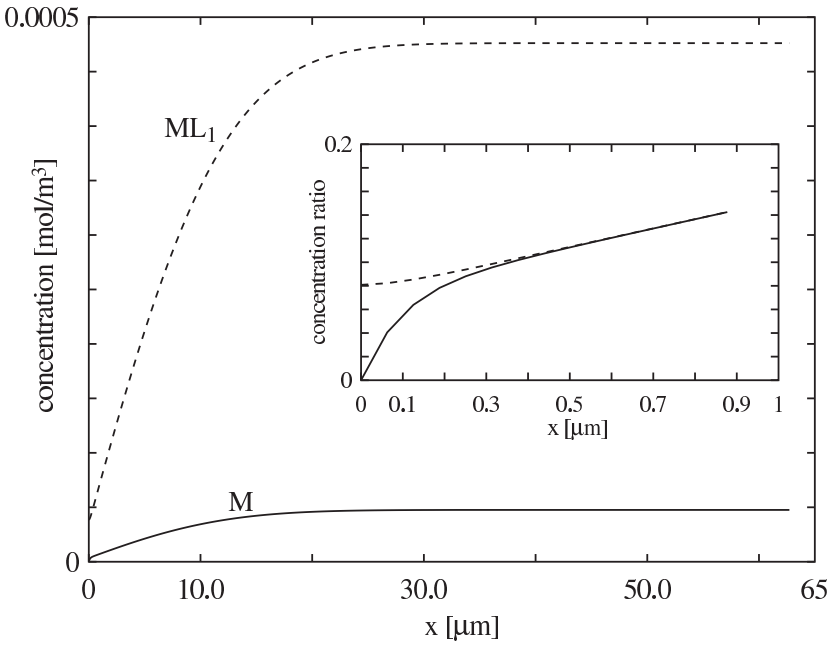

Figure 9: Two complexes, ML_1 and ML_2 with ligand excess. Concentration profiles of M and ML_1 as a function of the distance x from the electrode surface. The concentration ratio depicted in the inset is defined as c_X/c_X^* for X=M and ML_1. Other parameters are as in figure 8. The reaction layer thickness for the reaction $M + L_1 \rightleftharpoons ML_1$ is $\mu_1 = 0.1\mu m$. The profile concentrations of L_1, L_2 and ML_2 are not shown because they are constant due to the excess of L_1 and L_2 and the very low dynamics of ML_2.

Published in Physical Chemistry Chemical Physics 2005, vol 7, p 3331-33-41
DOI: 10.1039/b505890b reprints also to galceran@quimica.udl.cat

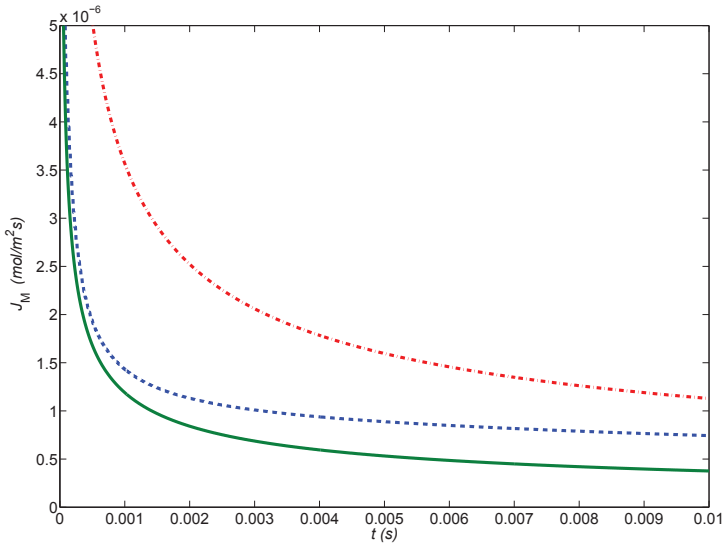

Figure 10: One complex, ML, without excess of ligand. Flux of metal M at $x = 0$ by using the RD scheme, in the following conditions: $K = 100 m^3/mol$, $k_a = 10^4 m^3/mol \cdot s$, $D_M = D_L = D_{ML} = 10^{-10} m^2/s$, $c^*_{M,tot} = 0.02 mol/m^3$, $c^*_L = 0.02 mol/m^3$, $\Delta t = 0.01 ms$, $\omega_M = \omega_L = \omega_{ML} = 1.98$, $\Delta x = 0.18 \mu m$. The analytical solution for the flux in the labile case, shown for comparison, is valid only in presence of excess of ligand. Dashed-dotted line (-.): labile complex, eq. (48); solid line (-): inert complex, eq. (47); dashed line (–): numerical solution.

Published in Physical Chemistry Chemical Physics 2005, vol 7, p 3331-33-41
DOI: 10.1039/b505890b reprints also to galceran@quimica.udl.cat

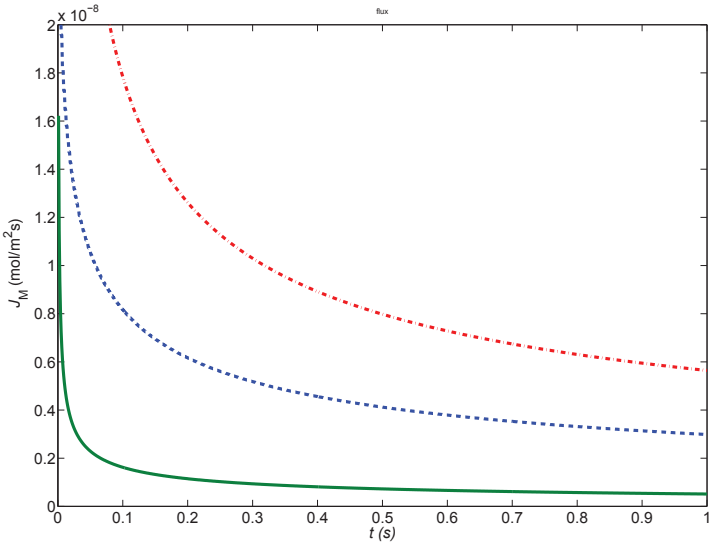

Figure 11: Two complexes, ML_1 and ML_2, without ligand excess. Parameters: $D = 10^{-10} m^2/s$ for all the species, $k_a^{(1)} = 10^6 mol^{-1} m^3 s^{-1}$, $k_d^{(1)} = 10^2 s^{-1}$, $k_a^{(2)} = 10^{-2} mol^{-1} m^3 s^{-1}$, $k_d^{(2)} = 10^{-6} s^{-1}$, $c^*_{M,tot} = 10^{-3} mol/m^3$, $c^*_{L_1} = c^*_{L_2} = 5 \cdot 10^{-4} mol/m^3$, $c^*_{ML_1} = c^*_{ML_2} = 4.55 \cdot 10^{-4} mol/m^3$, $\Delta t = 10^{-3} s$, $\Delta x = 0.3 \mu m$, $n_x = 300$. The plot shows the flux computed with equation (28) (dashed line (–)) obtained by the numerical simulation of the RD scheme compared with the flux in the fully inert (solid line (-)) and labile (dashed-dotted (-.)) complexes in excess of ligands, equations (47) and (48) respectively.

Published in Physical Chemistry Chemical Physics 2005, vol 7, p 3331-33-41
DOI: 10.1039/b505890b reprints also to galceran@quimica.udl.cat

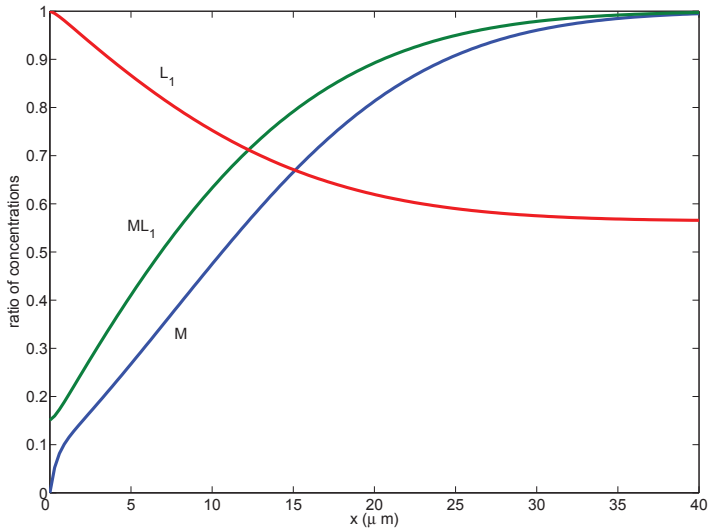

Figure 12: Two complexes, ML_1 and ML_2, without ligand excess. Normalised concentration profiles of M, ML_1 and L_1, as a function of the distance from the electrode. Other parameters as in figure 11. The reaction layer thickness for the reaction $M + L_1 \rightleftharpoons ML_1$ is $\mu_1 = 0.45\mu m$. The normalised concentration profiles of L_2 and ML_2 are not shown because they are horizontal and equal to 1.0, due to the very low dynamics of ML_2.

Published in Physical Chemistry Chemical Physics 2005, vol 7, p 3331-33-41
DOI: 10.1039/b505890b reprints also to galceran@quimica.udl.cat

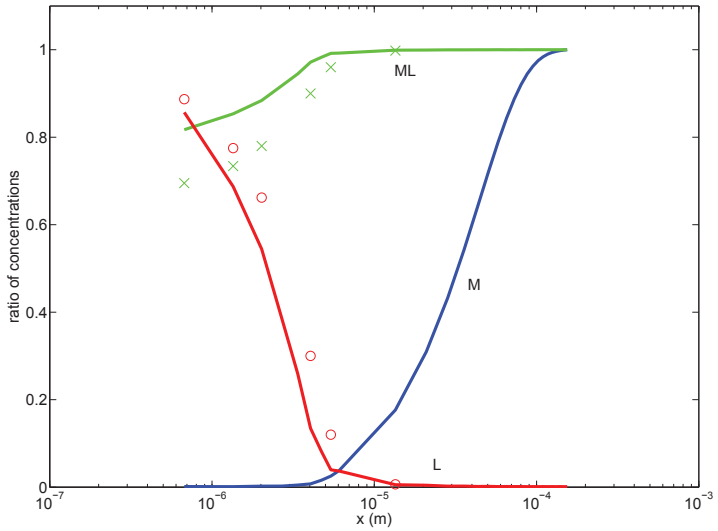

Figure 13: One complex ML in non excess of ligand. Normalised concentration profiles corresponding to $k_{\mathrm{a}} = 10^{8} mol^{-1} m^{3} s^{-1}$, $k_{\mathrm{d}} = 500 s^{-1}$,$\mu = 0.7 \mu m$, $c^{*}_{\mathrm{M,tot}} = 0.1 mol \cdot m^{-3}$, $c^{*}_{\mathrm{L,tot}} = 0.08 mol \cdot m^{-3}$, $t = 1s$, $D_{\mathrm{M}} = 10^{-9} m^{2}/s$, $D_{\mathrm{ML}} = D_{\mathrm{L}} = 10^{-10} m^{2}/s$, $\Delta t = 10^{-4} s$, $\Delta x = \mu$. Profiles of M, ML and L correspond to the ratios $c_{\mathrm{M}}/c^{*}_{\mathrm{M}}$, $c_{\mathrm{ML}}/c^{*}_{\mathrm{ML}}$ and $c_{\mathrm{L}}/c_{\mathrm{L}}(0)$, respectively. Continuous lines are obtained by numerical simulations using the RD scheme. Circles (o) and crosses (+) correspond to the values of L and ML shown in figure 7 of [17].

Published in Physical Chemistry Chemical Physics 2005, vol 7, p 3331-33-41
DOI: 10.1039/b505890b reprints also to galceran@quimica.udl.cat

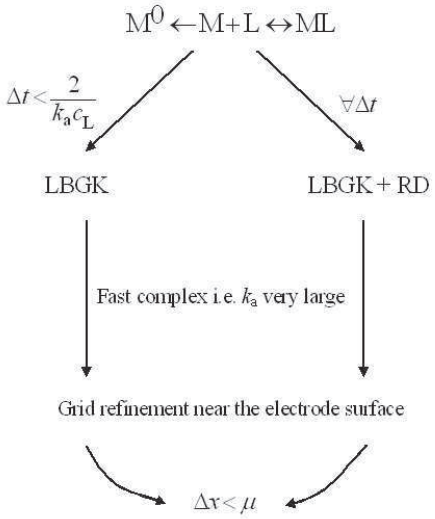

Figure 14: Memorandum of the application of the numerical schemes proposed. The LBGK scheme, equation (20), is convergent only under a time condition $\Delta t < 2/k_{\mathrm{a}}c_{\mathrm{L}}$, while by using the splitting scheme RD the convergence is ensured for any time step Δt. On the other hand, both NS and RD schemes need a grid refinement near the electrode, because Δx must be less than the reaction layer thickness μ, which is inversely proportional to $k_{\mathrm{a}}^{1/2}$.